arXiv:2610.40473v1 [eess.SY] 29 Oct 2026

Fundamental Limits of Sampling-Based Reachability: Geometry and Flow Distortion

Jixian Liu, Ihab Tabbara, Hussein Sibai, and Enrique Mallada

***Abstract*—Sampling-based reachability estimates reachable sets from finitely many simulated trajectory endpoints. Existing guarantees often control missed probability mass or approximation error relative to the convex hull of the reachable set, leaving the geometric error relative to the reachable set incompletely characterized. We study this error as a problem of support estimation under flow distortion. Our assumptions combine a uniform lower bound on the local volume density of the initial set, a lower bound on the sampling density, and a one-sided Lipschitz constant μ for the vector field. These conditions admit initial sets with corners and dynamics that may expand or contract. In the fine-accuracy regime, $\tilde{\mathcal{O}}\big(2^n e^{n\mu T}(R/r)^n/(\rho\kappa)\big)$ independent endpoint samples suffice for Hausdorff accuracy r using the endpoint cloud. Here, n is the state dimension, T is the horizon, R is the volume-equivalent radius, and ρ and κ quantify sampling density and local volume density. For $n \geq 2$ and sufficiently small κ, a minimax lower bound over all estimators based only on independent endpoints matches these dependencies up to a dimension-dependent factor $2 \cdot 4^n$ and logarithmic factors, within the stated parameter range and when the state domain accommodates the construction. The exponential burden in dimension, and in the horizon for expanding systems, is therefore intrinsic to this observation model. Planar experiments illustrate the predicted effects of corners and contraction; robot-arm experiments show how empirical accuracy deteriorates with dimension.**

***Index Terms*—Hausdorff distance, one-sided Lipschitz systems, reachability analysis, sampling-based methods.**

I. Introduction

REACHABILITY analysis is a basic tool for certifying the safety of dynamical and learning-enabled systems [2]–[5]. Classical methods based on Hamilton–Jacobi equations [6], [7] or on set propagation [8], [9] give deterministic guarantees but scale poorly with the state dimension, and can be difficult to apply when the dynamics include learned components. Sampling-based methods instead propagate finitely many initial states through the dynamics and build the estimate from the resulting endpoints [10]–[16]. These methods require only trajectory simulation and are readily parallelized. They form part of a broader effort to exploit sampling and parallel computation in control and optimization, ranging from model predictive path integral control [17] to diffusion-style trajectory optimizers [18]–[21].

Two common types of approximation guarantee accompany these methods. The first bounds the probability mass or volume that the estimator fails to cover [10], [13], [22], but may allow a thin or spatially separated part of the reachable set to be missed entirely. The second controls the Hausdorff distance to the convex hull of the reachable set [11], [12], [23], which fills holes and merges components. In the conference version of this work [1], we cast the problem as geometric support estimation under flow distortion. Under positive reach of the closed exterior of the initial set, an L-Lipschitz vector field, and a sampling density bounded below, that work establishes finite-sample Hausdorff guarantees and a minimax lower bound of order $(e^{LT}/r)^n$. The lower bound shows that exponential dependence on the dimension n and horizon T can be intrinsic to the endpoint observation model.

Nevertheless, two features of that analysis limit its scope. First, $\operatorname{reach}((\operatorname{int} S_0)^c) \geq r_0$ requires every point of S_0 to lie in a ball of radius r_0 inside S_0, which is violated as soon as S_0 has an outward corner, that is, a nonsmooth boundary point with a tangent cone of aperture smaller than a half-space, such as a polytope vertex or a convex edge; such corners are ubiquitous among the initial sets used in practice. Inward (reflex) corners, by contrast, are admissible, since a locally convex closed exterior does not create the same obstruction. Second, the Lipschitz constant L is a two-sided worst-case quantity: it does not distinguish a contracting from an expanding system, although in the former the reachable set shrinks and estimating it should become easier, not harder, as the horizon grows.

Contributions: We address both limitations for autonomous systems $\dot{x} = F(x)$, estimating $S_T = \mathcal{R}_T(S_0)$ from trajectory endpoints over a family specified by the initial-set scale and geometry, the dynamics, and the sampling law. Our contributions are as follows.

- **Generality.** We identify conditions that convert local probability bounds into geometric coverage: (κ, λ)-standardness of the initial set, which gives a positive lower bound on its local volume density; one-sided Lipschitz continuity of the dynamics with constant μ; and a relative lower bound ρ on the sampling density. These conditions are sufficient for a uniform rate, though not necessary for consistency. The geometric assumption includes every full-dimensional convex polytope, with κ given by its smallest vertex solid angle, as well as closures of bounded open sets whose complements have

This paper extends the CoRL 2026 version [1]. This work was supported by the NSF Global Centers program under Grant No. 2330450, by the DOE Office of Science (ASCR) under Award No. 826565, and by the Amazon AI PhD Fellowship. All code and related materials are available at https://github.com/JeanLew01/reachapprox.

J. Liu and E. Mallada are with the Department of Electrical and Computer Engineering, Johns Hopkins University, Baltimore, MD, USA (e-mail: jliu376@jhu.edu; mallada@jhu.edu).

I. Tabbara and H. Sibai are with the Department of Computer Science and Engineering, Washington University in St. Louis, St. Louis, MO, USA (e-mail: i.k.tabbara@wustl.edu; sibai@wustl.edu).

positive reach, while the dynamical assumption accommodates both expansion and contraction.

- **Sample complexity.** We prove a random-covering upper bound: $\tilde{\mathcal{O}}\big((2e^{\mu T}R/r)^n/(\rho\kappa)\big)$ endpoint samples suffice for r-accurate inner coverage in the fine-accuracy regime, where R is the volume-equivalent radius of the initial set. With an estimator-dependent outer-deviation condition, this yields a Hausdorff guarantee, and contraction provably reduces the sampling burden.
- **Unavoidability.** For $n \geq 2$ and sufficiently small κ, we establish a minimax lower bound under the scale and domain conditions of Theorem 2: every estimator based only on i.i.d. endpoints requires, in the worst case, $\widetilde{\Omega}\big((e^{\mu T}R/(2r))^n/(\rho\kappa)\big)$ samples. Hence, the dependence on the dimension, time horizon, target accuracy, initial-set scale, sampling density and local volume density is unavoidable for sampling-based reachability from endpoints. In particular, the required number of samples grows exponentially with the dimension n, since $e^{\mu T}R/(2r) > 8$ wherever the lower bound applies. The upper and lower bounds agree in all these factors up to the constant $2 \cdot 4^n$ and logarithmic factors.
- **Numerical experiments.** On planar systems with closed-form flows, including a vector field that is one-sided Lipschitz but not globally Lipschitz, the measured Hausdorff error follows the predicted dependence on the corner angle of the initial set, on μ rather than on the Lipschitz constant, and on the horizon through the factor $e^{\mu T}$. On a multi-link MuJoCo robotic arm, the sample complexity degrades with the state dimension, and adversarial sampling improves accuracy at larger budgets, while the fitted convergence rate still deteriorates with dimension.

Notation: All norms are Euclidean and all logarithms are natural. $|A|$ is Lebesgue measure, $\operatorname{int} A$ and ∂A are interior and boundary, and $A^c := \mathbb{R}^n \setminus A$. $\mathcal{B}_r(x)$ is the closed ball, $\mathcal{B}_r := \mathcal{B}_r(0)$ and $\omega_n := |\mathcal{B}_1|$. $d(x, A) := \inf_{a\in A} \|x - a\|$, $\mathcal{B}_r(A) := \{x : d(x, A) \leq r\}$, d_H is the Hausdorff distance and conv the convex hull. The covering number $\mathcal{N}(A, h)$ is the smallest number of closed balls of radius h centered in A whose union contains A. The symbols $\tilde{\mathcal{O}}$ and $\tilde{\Omega}$ hide logarithmic factors. For $m \geq 0$, $\mathbb{S}^m := \{z \in \mathbb{R}^{m+1} : \|z\| = 1\}$ is the unit sphere and σ_m is its m-dimensional surface measure, with σ_0 the counting measure on $\mathbb{S}^0 = \{-1, 1\}$. For a nonempty closed set C, $\operatorname{reach}(C)$ is the supremum of the radii a such that every point at distance less than a from C has a unique nearest point in C. For a regular closed set $S = \overline{\operatorname{int} S}$, its closed exterior is $(\operatorname{int} S)^c$. Reach assumptions below concern this closed exterior, or the closed complement A^c of an explicitly specified open set A.

II. Preliminaries and Problem Statement

We consider an autonomous continuous-time dynamical system $\dot{x} = F(x)$ on a state domain $\mathcal{X} \subseteq \mathbb{R}^n$, $n \in \mathbb{N}_+$, with a one-sided Lipschitz vector field $F : \mathcal{X} \to \mathbb{R}^n$. Given an initial condition $x_0 \in \mathcal{X}$, let $\varphi(t, x_0)$ denote the solution at time $t \geq 0$, and write $\varphi_T := \varphi(T, \cdot)$. For a compact initial set $S_0 \subseteq \mathcal{X}$ and a time horizon $T \geq 0$, the forward reachable set is

$$\mathcal{R}_T(S_0) := \{\varphi(T, x_0) \in \mathcal{X} : \ x_0 \in S_0\}.$$

Write $S_T := \mathcal{R}_T(S_0)$. We estimate S_T from endpoints $Y_i := \varphi_T(X_i)$, $i = 1, \ldots, N$, where $X_1, \ldots, X_N$ are independent and identically distributed (i.i.d.) samples from a probability distribution P_0 with $\operatorname{supp}(P_0) = S_0$. Under our standing assumptions, φ_T is continuous (Lemma 3). Consequently, the endpoints are i.i.d. samples from the pushforward distribution $P_T := (\varphi_T)_{\#}P_0$, with $\operatorname{supp}(P_T) = \varphi_T(S_0) = S_T$ by continuity and compactness. A sampling-based reachable-set estimator is a measurable random closed set $\widehat{S}_N = \widehat{S}_N(Y_1, \ldots, Y_N) \subseteq \mathbb{R}^n$. We require both directed distance losses, and hence $d_H(S_T, \widehat{S}_N)$, to be Borel measurable for every fixed target S_T. The Hausdorff loss is $+\infty$ for empty or unbounded estimates. Estimators may depend on the family parameters but, in the endpoint observation model, have no instance-specific information beyond the endpoints.

Probabilistic coverage is a common performance criterion in sampling-based and learning-based reachability analysis. A typical result guarantees $P_T(S_T \setminus \widehat{S}_N) \leq \varepsilon$ with confidence at least $1 - \delta$ for an estimate $\widehat{S}_N$ built from independent endpoints [22]. Such a guarantee bounds the probability mass of the omitted states, but not their distance from the estimated set: a region carrying little mass under P_T may extend far beyond $\widehat{S}_N$, so a small coverage error can coexist with a large Hausdorff distance. This discrepancy is consequential for safety verification, because rarely reached states may still violate constraints and thereby invalidate a certificate.

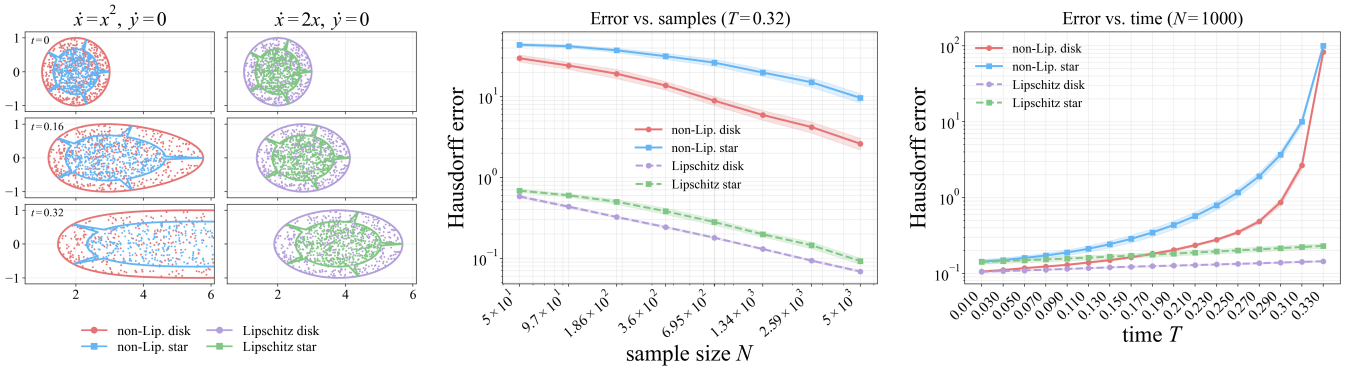
To address this gap, we seek finite sample-size bounds that suffice to approximate the reachable set to a specified target Hausdorff distance with high probability, together with minimax lower bounds showing that their dependence on the problem parameters cannot be improved in the worst case, up to dimension-dependent constants and logarithmic factors. Specifically, given an accuracy tolerance $r > 0$ and a confidence level $1 - \delta$, we characterize conditions on the problem instance and the sample size N that ensure

$$P_T^N\left(d_H(S_T, \widehat{S}_N) \leq r\right) \ \geq \ 1 - \delta.$$

Unlike a bound on missed probability mass, this guarantee ensures that every point in either set lies within distance r of the other. It controls both omissions that may undermine safety verification and overapproximation that may cause unnecessary conservatism.

A connection between missed probability mass and inner geometric error requires a lower bound on $P_T(\mathcal{B}_r(x))$ uniform in $x \in S_T$. Indeed, if $d(x, \widehat{S}_N) > r$, then $\mathcal{B}_r(x)$ is disjoint from $\widehat{S}_N$, so its entire mass is omitted. A separate outer-deviation condition is needed to control points of the estimate that lie far from S_T.

Fig. 1 illustrates how initial-set geometry and flow distortion affect the accuracy of sampling-based reachable-set estimation. In panel (a), the same disk and star are propagated under two planar fields. The left column uses the quadratic field $\dot{x} = x^2$, $\dot{y} = 0$, whose flow exhibits unbounded stretching as the finite blow-up time is approached. The right column



(a) Reachable sets and samples (b) Error vs. sample size (c) Error vs. horizon

Fig. 1. Geometry and dynamics. (a) A disk and a nonconvex star of comparable diameter, the latter the union of a circular core of radius $2/3$ of the disk radius and five 15° corners, propagated under two fields. Left: $\dot{x} = x^2$, $\dot{y} = 0$, which is not globally Lipschitz and blows up in finite time; the right tip of the reachable set escapes as $t \uparrow 1/3$, and the panel is clipped. Right: the linear field $\dot{x} = 2x$, $\dot{y} = 0$, which is Lipschitz, hence one-sided Lipschitz, and maps the disk to an ellipse. Rows: $t = 0$, 0.16, and 0.32. Dots: 500 samples, drawn uniformly by area on each initial set; curves: the exact reachable boundaries. (b) Mean Hausdorff error of the endpoint cloud against $N \in [5 \times 10^1, 5 \times 10^3]$ at $T = 0.32$, and (c) against T at $N = 1000$; bands: 95% confidence intervals over 50 trials. Time changes the distortion of neighborhoods, while the geometry of S_0 changes the local area fraction, and hence the local sampling probability, even at a fixed horizon.

uses the linear field $\dot{x} = 2x$, $\dot{y} = 0$, under which the disk becomes an ellipse and the reachable set remains bounded at every finite horizon. Comparing the disk and the star highlights the effect of initial-set geometry, while comparing the two fields reveals the effect of flow distortion. Panels (b) and (c) quantify the Hausdorff error of the endpoint cloud. At a fixed horizon, the star yields larger errors than the disk for every tested sample size under both fields. Under the quadratic field, the star also has a shallower log–log decay slope, so its error decreases more slowly with sample size than that of the disk. With N fixed, the error grows sharply as $t \uparrow 1/3$ under the quadratic field, whereas under the linear field its logarithm grows approximately linearly with time. These observations highlight how dynamics and geometry determine local sampling probabilities. A one-sided Lipschitz bound μ controls the separation of trajectories by the factor $e^{\mu T}$, whereas the stretching under the quadratic field diverges as its blow-up time is approached. Geometry determines the local volume available for sampling: the 15° corners of the star occupy the fraction $\frac{15}{360} = \frac{1}{24}$ of sufficiently small disks centered at their tips, whereas the corresponding fraction at the smooth boundary of the disk tends to $\frac{1}{2}$ [1]. Under uniform sampling, neighborhoods of these sharp corners therefore carry less probability mass and are harder to resolve. More generally, a sampling-density lower bound prevents regions of positive volume from carrying arbitrarily little mass. These observations motivate conditions on the dynamics, initial-set geometry, and sampling density, which we introduce after stating a well-posedness assumption.

Assumption 1 (Well-posedness): For every instance and horizon T considered, $\varphi(t, \cdot)$ is well defined and unique on S_0 and $\varphi(t, S_0) \subseteq \mathcal{X}$ for all $t \in [0, T]$.

To state the geometric condition, we recall the notion of a standard set [24], [25].

Definition 1 ((κ, λ)-standard set): A compact set $S_0 \subset \mathbb{R}^n$ is (κ, λ)-*standard*, $\kappa \in (0, 1]$, $\lambda > 0$, if

$$|\mathcal{B}_r(x) \cap S_0| \ \geq \ \kappa\, \omega_n r^n \qquad \forall x \in S_0,\ r \in (0, \lambda]. \quad (1)$$

Standardness is a condition on local volume alone. Proposition 2 in Appendix A-F gives three classes: closures $\overline{A}$ of open sets with $\mathrm{reach}(A^c) \geq r_0 > 0$ are $(2^{-n}, r_0)$-standard; uniform inner-cone sets with half-angle α are standard with $\kappa = \vartheta_n(\alpha)$, the fraction of the unit ball occupied by the cone; and convex polytopes and their finite unions are standard at an explicit scale, with κ determined by their vertex solid angles.

Standardness controls the local thickness of S_0 by requiring it to occupy at least a fraction κ of every sufficiently small ball centered in S_0. It thereby excludes shapes such as outward cusps, whose local volume at the cusp decays faster than r^n, from the class for which the uniform rate r^{-n} is proved, although it does not preclude their consistent recovery at a slower rate. One-sided Lipschitz bounds, in turn, control how distances between trajectories evolve. We then combine these geometric and dynamical conditions with the sampling assumptions to define the following problem family.

Definition 2 (Problem family): Fix constants $R > 0$, $\mu \in \mathbb{R}$, $\kappa \in (0, 1]$, $\lambda > 0$ and $\rho \in (0, 1]$. Let $\mathscr{F}^{\mathrm{std}}_{R,\mu,\kappa,\lambda,\rho}$ denote the class of triples (S_0, F, P_0) such that:

1) $S_0 \subset \mathcal{X}$ is a compact set with $|S_0| = \omega_n R^n$ and $|\partial S_0| = 0$;
2) S_0 is (κ, λ)-standard;
3) $F : \mathcal{X} \to \mathbb{R}^n$ is continuous, satisfies Assumption 1, and is one-sided Lipschitz with constant μ, i.e., $\langle F(x) - F(y), x - y\rangle \leq \mu\|x - y\|^2$ for all $x, y \in \mathcal{X}$;
4) P_0 is absolutely continuous with respect to the Lebesgue measure on $\mathbb{R}^n$, with density p_0, and satisfies $\mathrm{supp}(P_0) = S_0$ and $p_0(x) \geq \rho/|S_0|$ for a.e. $x \in S_0$.

The one-sided Lipschitz condition in item 3 is weaker than Lipschitz continuity: every L-Lipschitz field satisfies it with $\mu = L$, while the cubic field $F(x) = -\|x\|^2 x$ satisfies it with $\mu = 0$ without being globally Lipschitz (Section IV-B).

Three features of Definition 2 merit comment. First, for bounded S_0 with $|\partial S_0| = 0$, taking its closure preserves its volume and absolutely continuous sampling law. If the flow extends continuously to this closure, it also preserves

the Hausdorff approximation error. We therefore work with compact S_0. The null-boundary condition holds for Lipschitz domains, convex bodies, and finite unions of polytopes. Second, items 1 and 2 impose a quantitative nondegeneracy condition on S_0: every ball $\mathcal{B}_r(x)$ with $x \in S_0$ and $r \le \lambda$ satisfies $|\mathcal{B}_r(x) \cap S_0| \ge \kappa\,\omega_n r^n > 0$. Here, R is the radius of a ball with the same volume as S_0, while ρ specifies the sampling-density lower bound relative to the uniform distribution on S_0. Third, the density bound in item 4 is required only almost everywhere, because p_0 is determined by P_0 only up to Lebesgue-null sets; in particular, modifying p_0 on ∂S_0 leaves P_0 unchanged. The proofs use the lower bound only in its integrated form: $P_0(A) \ge \frac{\rho}{|S_0|}\,|A \cap S_0|$ for every measurable set A. The geometric parameters (κ, λ) and the dynamical bound μ determine how this initial density translates into probability mass in neighborhoods of the reachable set. In the next section, we quantify this relationship to establish sample-complexity upper bounds and compare them with minimax lower bounds.

III. Reachable Set Approximation under Regular Geometry

For the problem family defined above, we study the approximation of the reachable set in Hausdorff distance from finitely many endpoint samples. Our main tool is a local lower bound on endpoint probabilities, derived from the standardness of S_0, the lower bound on the initial density, and distortion estimates for the flow induced by the one-sided Lipschitz condition. This estimate yields an inner-coverage sample-complexity bound for any estimator that contains all observed endpoint samples. A full Hausdorff-error guarantee additionally requires an estimator-specific outer-deviation bound. Finally, we show that the r^{-n} scaling is information-theoretically unavoidable, and so is the dependence on $(\rho\kappa)^{-1}$ for every sufficiently small κ when the domain accommodates the lower-bound construction.

A. Local Mass Bounds under Flow Distortion

Standardness provides a lower bound on the volume of every small ball centered in S_0, which the density assumption in Definition 2 converts into a lower bound on its mass under P_0. To carry this local-mass bound to the reachable set at time T, we do not track the standardness of S_T itself. Instead, we propagate the local thickness of S_0 through the flow, whose distortion is controlled by the one-sided Lipschitz constant: the preimage of an r-neighborhood centered on the reachable set contains an initial neighborhood of radius $s = e^{-\mu T} r$, whose probability mass is controlled by the local volume bound. This yields, at every scale, the local lower bound on endpoint probabilities and the covering bound used in the sampling argument of the next subsection.

Lemma 1 (Endpoint local probability lower bound): Let $(S_0, F, P_0) \in \mathscr{F}^{\mathrm{std}}_{R,\mu,\kappa,\lambda,\rho}$. Then, for every $y \in S_T$ and every $r > 0$,

$$P_T\big(\mathcal{B}_r(y) \cap S_T\big) \;\ge\; \rho\,\kappa\Big(\frac{\min\{e^{-\mu T} r,\ \lambda\}}{R}\Big)^n. \tag{2}$$

Proof: See Appendix A-B. ∎

The preceding lemma bounds the probability mass of individual neighborhoods from below. To translate this local coverage into a uniform coverage guarantee for S_T, we also need to bound the number of such neighborhoods required to cover the reachable set. The following lemma provides this bound.

Lemma 2 (Covering number of the reachable set at every scale): Let $(S_0, F, P_0) \in \mathscr{F}^{\mathrm{std}}_{R,\mu,\kappa,\lambda,\rho}$. Then, for every $r > 0$,

$$\mathcal{N}(S_T, r) \;\le\; \frac{R^n}{\kappa\,\min\{\frac{1}{2}e^{-\mu T} r,\ \lambda\}^n}. \tag{3}$$

Proof: See Appendix A-B. ∎

B. Sample Complexity Bounds

Lemma 1 shows that every r-neighborhood centered on the reachable set carries endpoint probability mass at least $\rho\kappa(e^{-\mu T} r/R)^n$ for $r \le e^{\mu T}\lambda$, and at least $\rho\kappa(\lambda/R)^n$ beyond that scale. We use this bound to determine how many endpoints suffice for inner coverage at any accuracy $r > 0$. The argument is estimator-agnostic: it requires only that the estimator contain all sampled endpoints. The resulting bound depends on r and T only through the *preimage scale*

$$\varrho_T(r) := \min\{\tfrac{1}{2}e^{-\mu T} r,\ \lambda\},$$

the radius of initial neighborhoods $\mathcal{B}_{\varrho_T(r)}(x) \cap S_0$ that φ_T maps into balls of radius $r/2$ (Lemma 3), capped at the scale λ up to which standardness controls the local volume.

Theorem 1 (Sampling upper bound for inner coverage): Let $(S_0, F, P_0) \in \mathscr{F}^{\mathrm{std}}_{R,\mu,\kappa,\lambda,\rho}$, let $Y_1, \dots, Y_N$ be i.i.d. samples from P_T, and suppose that the estimator $\widehat{S}_N$ contains all endpoint samples, i.e., $Y_i \in \widehat{S}_N$ for $i = 1, \dots, N$. Set $D_0 := \mathrm{diam}(S_0)$. For $r > 0$ and $\delta \in (0,1)$, if N satisfies any of the following sufficient conditions, then $\sup_{x \in S_T} d(x, \widehat{S}_N) \le r$ with probability at least $1 - \delta$.

1) *Fine regime,* $0 < r \le 2e^{\mu T}\lambda$: $N \ge N_{\mathrm{fine}}(r, \delta)$, where
$$N_{\mathrm{fine}}(r,\delta) := \frac{2^n e^{n\mu T} R^n}{\rho\kappa r^n}\Big[\log\frac{2^{2n} e^{n\mu T} R^n}{\kappa r^n} + \log\frac{1}{\delta}\Big]. \tag{4}$$
2) *Saturated regime,* $2e^{\mu T}\lambda < r < e^{\mu T} D_0$: $N \ge N_{\mathrm{sat}}(\delta)$, where
$$N_{\mathrm{sat}}(\delta) := \frac{1}{\rho\kappa}\left(\frac{R}{\lambda}\right)^n\Big[\log\frac{2^n R^n}{\kappa\lambda^n} + \log\frac{1}{\delta}\Big]. \tag{5}$$
3) *Trivial regime,* $r \ge e^{\mu T} D_0$: one sample suffices, i.e., every $N \ge 1$ works.

Proof: See Appendix A-C. ∎

The covering step follows the standard argument of support estimation [24], [26]; the new ingredient is the flow-distortion reduction.

Corollary 1 (Convex initial sets: no saturation): Let $(S_0, F, P_0) \in \mathscr{F}^{\mathrm{std}}_{R,\mu,\kappa,\lambda,\rho}$, assume that $\widehat{S}_N$ contains all sampled endpoints and that S_0 is convex, and set $D := \mathrm{diam}(S_0)$. Then S_0 is $((R/D)^n, D)$-standard. Hence, Theorem 1 holds for every $r > 0$ and $\delta \in (0,1)$ provided that

$$N \ge \frac{1}{\rho}\left(\frac{D}{\varrho'_T(r)}\right)^n\left[n\log\frac{2D}{\varrho'_T(r)} + \log\frac{1}{\delta}\right], \tag{6}$$

$$\varrho'_T(r) := \min\{\tfrac{1}{2}e^{-\mu T}r, D\}. \tag{7}$$

Proof: See Appendix A-C. ∎

In (6), the geometric dependence is expressed through the diameter: substituting $\kappa' = (R/D)^n$ and $\lambda' = D$ into the upper bound gives the prefactor $\rho^{-1}(D/\varrho'_T(r))^n$ and the logarithmic term $n\log(2D/\varrho'_T(r))$.

Remark 1 (Saturation and convexity): The plateau in (5) reflects the scale λ up to which standardness is known. Once $\varrho_T(r) = \lambda$, the local-mass argument no longer improves as r increases. For general standard sets, separated components can produce a genuine plateau, as in Section IV-C. This does not establish a matching minimax lower bound in the saturated regime.

For convex S_0, standardness extends to $D = \operatorname{diam}(S_0)$ with constant $(R/D)^n$. Thus, (6) improves throughout the nontrivial range $r < e^{\mu T}D$; at $r \geq e^{\mu T}D$, one endpoint already suffices. No saturated interval is needed for this convex-set guarantee.

Corollary 2 (Hausdorff bound with outer deviation): Under the assumptions of Theorem 1, suppose additionally that the estimator satisfies the outer-deviation condition $\widehat{S}_N \subseteq \mathcal{B}_\eta(S_T)$ almost surely for some deterministic $\eta \geq 0$. Then, with probability at least $1-\delta$, $d_H(S_T, \widehat{S}_N) \leq \max\{r, \eta\}$.

Proof: See Appendix A-C. ∎

Remark 2 (Estimator-dependent outer deviation): The condition $\widehat{S}_N \subseteq \mathcal{B}_\eta(S_T)$ is equivalent to $\sup_{z\in\widehat{S}_N} d(z, S_T) \leq \eta$. In Corollary 2, Theorem 1 controls the directed error from S_T to $\widehat{S}_N$, while η controls the opposite direction. For an inner estimator that contains all endpoints, $\eta = 0$; for a union of balls of radius h centered at the endpoints, $\eta = h$; and for the convex hull of the endpoints, $\eta = \sup_{z\in\operatorname{conv}(S_T)} d(z, S_T)$.

We next establish a lower bound that applies to every measurable estimator based on i.i.d. endpoint samples. It shows that the dependence on r^{-n}, $1/\rho$ and $1/\kappa$ is unavoidable in dimensions $n \geq 2$ for every $\kappa \leq \kappa_n$ under the domain condition below, where

$$\kappa_n := \frac{|K_n \cap \mathcal{B}_1|}{\omega_n} \text{ and } K_n := \Big\{v \in \mathbb{R}^n : \ v_1 \geq \tfrac{1}{\sqrt{2}}\|v\|\Big\}. \tag{8}$$

The constant κ_n is the fraction of the unit ball $\mathcal{B}_1$ occupied by the circular cone K_n with apex at the center and half-angle $\pi/4$; it is the standardness constant of such a cone at its apex. One has $\kappa_2 = \frac{1}{4}$, $\kappa_3 = \frac{1}{2}\big(1 - \frac{1}{\sqrt{2}}\big) \approx 0.146$ and $\kappa_4 \approx 0.091$, and $\kappa_n \geq 2^{-n}$ for every $n \geq 2$, with equality only for $n = 2$ (Remark 5). The range $\kappa \leq \kappa_n$ therefore contains every $\kappa \leq 2^{-n}$, the local volume density that positive reach guarantees.

Theorem 2 (Minimax lower bound): Let $n \geq 2$, $R > 0$, $\mu \in \mathbb{R}$, $T \geq 0$, $\rho \in (0, 1]$, $\delta \in (0, \frac{1}{2})$, $0 < r < e^{\mu T}R/16$, $0 < \kappa \leq \kappa_n$ and $0 < \lambda \leq 3R/32$. Suppose $\mathcal{B}_{3R\max\{1,e^{\mu T}\}}(c) \subseteq \mathcal{X}$ for some $c \in \mathbb{R}^n$, and define

$$N_{\mathrm{lb}}(r, \delta) := \frac{1}{2\rho\kappa}\Big(\frac{e^{\mu T}R}{2r}\Big)^n \log\frac{1}{2\delta}. \tag{9}$$

If $N < N_{\mathrm{lb}}(r, \delta)$, then for every measurable estimator $\widehat{S}_N$ there exists an instance $(S_0, F, P_0) \in \mathscr{F}^{\mathrm{std}}_{R,\mu,\kappa,\lambda,\rho}$ such that

$$P_T^N\big(d_H(\widehat{S}_N, S_T) > r\big) > \delta.$$

Proof: See Appendix A-E. ∎

Remark 3 (Scope of the lower bound): Theorem 2 pertains to the i.i.d. endpoint model: its hard instances share the dynamics $F(x) = \mu(x - c)$ on $\mathcal{X}$ and differ only in S_0, so knowledge of the dynamics does not distinguish them. Algorithms that know both S_0 and F, adaptive sampling schemes, and model-aware methods lie outside its scope. The restriction $r < e^{\mu T}R/16$ comes from the two-tip construction, which needs tips separated by more than $2re^{-\mu T}$ inside a body of volume $\omega_n R^n$; whether the bound extends to coarser accuracies, where it would need instances of a different shape, is open.

The two instances differ only on a sector of radius about $2re^{-\mu T}$ at an apex of local volume fraction κ, whose probability can be chosen arbitrarily close to $\rho\kappa(2re^{-\mu T}/R)^n$ from above; up to the factor $\frac{1}{2}\log\frac{1}{2\delta}$, (9) is the inverse of that probability. The hard instances lie in the family, and the apex of the kept tip has local volume fraction exactly κ (Lemma 10(ii)); the bound says nothing about an individual set whose local volume fraction exceeds κ everywhere, such as a disk, whose error can be smaller.

Under the restrictions of Theorem 2 and the fine-regime condition $r \leq 2e^{\mu T}\lambda$, the upper bound (4), applied to the endpoint cloud, and the lower bound (9) have the same dependence on $e^{\mu T}R/r$, ρ and κ for every $\kappa \leq \kappa_n$, up to the factor $2 \cdot 4^n$ and logarithmic factors. This factor is itself exponential in n: both bounds exhibit exponential dependence on n and, when $\mu > 0$, exponential growth in T, but their bases differ by a factor of 4, so they do not pin down a sharp, dimension-uniform rate. The dependence on r^{-n}, $1/\rho$ and $1/\kappa$ is thus unavoidable in the sense of Theorem 2, while $e^{n\mu T}$ captures the effects of expansion and contraction. Table I summarizes the comparison.

TABLE I
SAMPLE-COMPLEXITY BOUNDS IN THE COMMON REGIME SPECIFIED ABOVE.

Bound	Range of κ	Sample complexity
Upper bound	$0 < \kappa \leq 1$	$\tilde{\mathcal{O}}\Big(\frac{1}{\rho\kappa}\Big(\frac{2e^{\mu T}R}{r}\Big)^n\Big)$
Lower bound	$0 < \kappa \leq \kappa_n$	$\Omega\Big(\frac{1}{\rho\kappa}\Big(\frac{e^{\mu T}R}{2r}\Big)^n \log\frac{1}{2\delta}\Big)$

IV. Numerical Experiments

Our experiments isolate the two ingredients of Section III that go beyond Liu et al. [1]: the factor $1/\kappa$, which stems from a regularity condition on the local volume of S_0 rather than on the shape of its boundary, a condition weaker than positive reach of the closed exterior; and the one-sided Lipschitz constant μ, which, unlike the Lipschitz constant $L \geq 0$, can be negative and therefore captures contraction. Sections IV-A and IV-B test each ingredient separately.

We then test the sample-complexity bounds that combine them. The upper bound of Theorem 1 and the lower bound of Theorem 2 depend on κ and μ through $e^{n\mu T}(R/r)^n/(\rho\kappa)$.

Section IV-C compares both bounds with the empirical sample complexity along the horizon.

These three experiments use planar systems with closed-form flows and explicit geometric parameters. A fourth experiment, on a multi-link robot arm, examines the dependence on the state dimension under uniform and adversarial sampling.

Setup of the planar experiments: The initial sets have area π and are sampled uniformly, so $R = 1$ and $\rho = 1$, and we take $\delta = 0.05$. We take the endpoint cloud $\widehat{S}_N = \{Y_1, \dots, Y_N\}$ as the estimator. It has $\eta = 0$ in Corollary 2, so that $d_H(S_T, \widehat{S}_N) = \sup_{x \in S_T} d(x, \widehat{S}_N)$, and every other estimator that contains the samples has an inner error at most as large. We approximate this distance using the endpoint Voronoi diagram and a discretization of ∂S_T. A maximum of the nearest-sample distance occurs either at an interior Voronoi vertex or on the boundary. For these smooth, invertible planar flows, membership is tested using φ_T^{-1} and the boundary is propagated from ∂S_0. The initial boundary spacing is at most 5×10^{-4}. For exact boundary samples, the resulting discretization error is at most $e^{\mu T} \times 5 \times 10^{-4}$; the interior Voronoi contribution is exact in exact arithmetic. Floating-point and polygonal boundary-approximation errors are additional numerical errors. Every condition is repeated over 200 independent trials. Three of the four vector fields are the linear fields

$$F_\mu(x) = \begin{bmatrix} \mu & -\omega \\ \omega & \mu \end{bmatrix} x, \qquad \omega = 4, \tag{10}$$

whose flow $\varphi_T(x) = e^{\mu T} \operatorname{Rot}(\omega T)\, x$ is a rotation composed with a scaling. Here $\operatorname{Rot}(\theta)$ denotes the counterclockwise planar rotation through angle θ. The one-sided Lipschitz constant of F_μ is μ, of either sign, whereas its Lipschitz constant is $L = (\mu^2 + \omega^2)^{1/2} \geq 4$.

A. Dependence on the Corner Angle

We take $\mu = -1$ and $T = 1$ in (10) and vary the initial set: the unit disk, for which $\operatorname{reach}((\operatorname{int} S_0)^c) = 1$; a square; isosceles triangles with apex angle $\theta \in \{60^\circ, 30^\circ, 15^\circ, 7.5^\circ\}$, for which $\kappa = \theta/(2\pi)$ by Proposition 2; and a translated copy of the closed cusp $\{0 \leq u \leq 3,\ |v| \leq \frac{\pi}{2}(u/3)^2\}$, which is not standard because its area in a disk of radius r centered at the origin scales as r^3. The middle panel of Fig. 2 shows the error for N from 30 to 10^5. The curves of all standard sets are parallel: over $N \geq 10^3$ their fitted log–log slopes lie between -0.46 and -0.49, which is the rate $N^{-1/n}$ of (4) up to its logarithm, and the corners of the square and of the triangles, which force the reach of their closed exteriors to vanish, do not degrade it. The cusp decays with slope -0.34, consistent with the rate $N^{-1/3}$ suggested by its local area scaling. These observations are consistent with the role of standardness in preserving the exponent despite corners. A corner does change the constant: the curves are ordered by κ, and at $N = 10^5$ the error of the 7.5° triangle is 1.7 times that of the disk.

The right panel isolates the corner effect at $N = 10^4$ by decreasing θ from 60° to 3.75°, or κ from $1/6$ to $1/96$. It shows the mean error and empirical 5–95% ranges, together with the upper bound and the minimax lower bound (9), both solved for r at $\delta = 0.05$. The lower curve is

$$r_{\mathrm{lb}}(N, \delta) = \frac{e^{\mu T} R}{2} \left(\frac{\log(1/(2\delta))}{2\rho\kappa N} \right)^{1/n}.$$

The plotted range satisfies $r_{\mathrm{lb}} < e^{\mu T} R/16$ and $\kappa \leq \kappa_2 = 1/4$. The lower bound concerns the family with standardness scale $\lambda_{\mathrm{lb}} = \min\{\lambda, 3R/32\}$, rather than either the mean or the quantile of the error for a fixed triangle.

For $\kappa \leq 1/48$, the mean Hausdorff error is within approximately 7% of the mean distance d_* from the propagated apex to the endpoint cloud. At radii s for which the pulled-back neighborhood remains within the apex cone, uniform sampling gives $\mathbb{P}(d_* > s) = [1 - \kappa(e^{-\mu T} s/R)^2]^N$. Including the four thinner triangles down to $\kappa = 1/384$ omitted from the figure, the fitted exponents of the mean and empirical 95% quantile with respect to κ are -0.49 and -0.51. For wider angles, the interior and edges contribute more strongly and the mean error levels off. Over the plotted range, the empirical 95% quantile is a factor of 3.2 to 4.4 below the upper bound and 2.8 to 3.9 above the minimax lower curve. For thin triangles, both the measured error and the bounds exhibit the $\kappa^{-1/2}$ dependence.

B. One-Sided versus Two-Sided Lipschitz Constants

TABLE II
HORIZON DEPENDENCE OF THE HAUSDORFF ERROR UNDER FOUR PLANAR VECTOR FIELDS.

Field	μ	L	rate	ratio	$e^{2\mu}$	e^{2L}
$F_{0.5}$	0.5	4.03	0.50	2.74	2.72	3.2×10^3
F_0	0	4.00	0.00	1.00	1	3.0×10^3
F_{-1}	-1	4.12	-1.00	0.134	0.135	3.8×10^3
cubic	0	35.4	—	0.256	1	5.8×10^{30}

In Table II, the rate is the least-squares slope of the logarithm of the mean error over $T \in [0, 2]$, and the ratio is the mean error at $T = 2$ divided by that at $T = 0$.

The initial set is the equilateral triangle of area π centered at $(2, 0)$, for which $(\kappa, \lambda) = (1/6, 0.778)$ and whose closed exterior has reach zero. We compare F_μ in (10) for $\mu \in \{0.5, 0, -1\}$ with the cubic damping field $F(x) = -\|x\|^2 x$, whose flow is $\varphi_T(x) = x/(1 + 2T\|x\|^2)^{1/2}$. This field is the negative gradient of a convex function, so $\mu = 0$, but it is not globally Lipschitz; on the ball that contains the trajectories its Lipschitz constant is $L = 35.4$.

For the three linear fields the error is exponential in T with fitted rates 0.50, 0.00 and -1.00, that is, with rate μ, although $L \approx 4$ for all of them (Fig. 3, middle, and Table II). A bound stated in terms of L predicts the growth e^{LT} for all three, a factor between 3.0×10^3 and 3.8×10^3 at $T = 2$, even for the sink, whose error actually decreases by the factor $0.134 \approx e^{-2}$. The upper bound of Theorem 1 follows each curve and stays a factor of about 3 above its 95% quantile over the whole horizon. For the cubic field, $\mu = 0$ gives a horizon-independent upper bound, even though no global Lipschitz constant exists. On the convex set S_0, the Jacobian of φ_T has tangential and

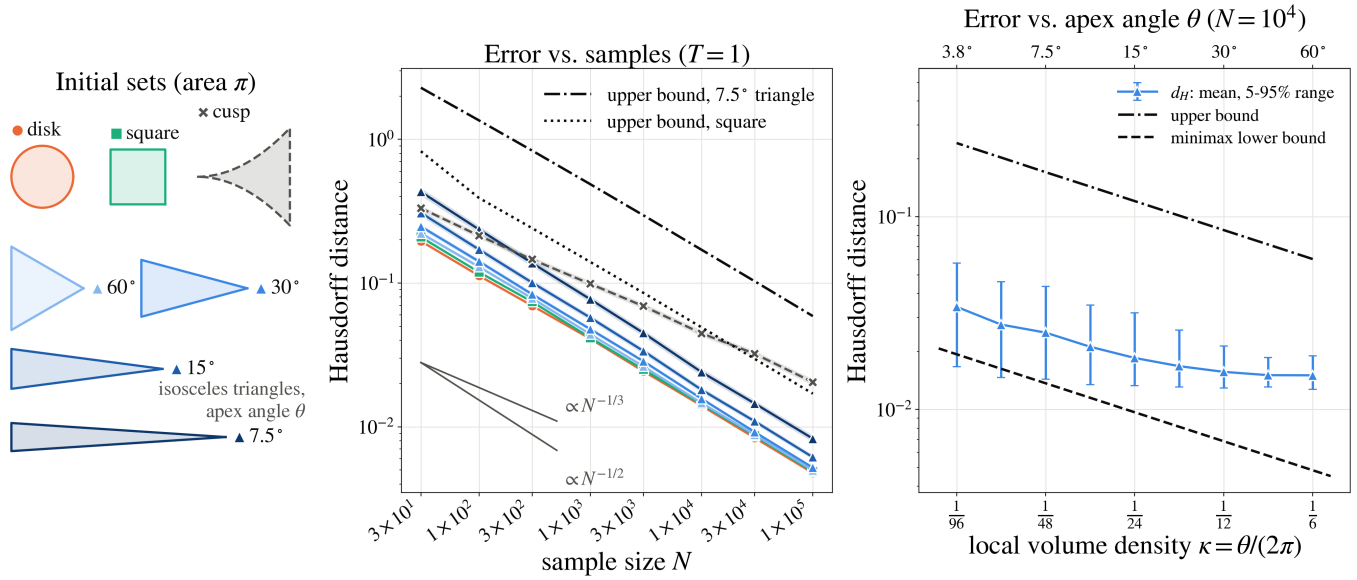


Fig. 2. Effect of the corner angle under the spiral sink F_{-1} at $T = 1$. Left: equal-area initial sets. Middle: mean Hausdorff error versus N, with 95% confidence bands and the upper bounds solved for r. Right: mean error and empirical 5–95% ranges at $N = 10^4$, together with the upper bound and the minimax lower bound (9) solved for r at $\delta = 0.05$. The lower curve is a worst-case bound over the admissible family of instances, not a bound on the mean or quantile of the error for each plotted triangle.

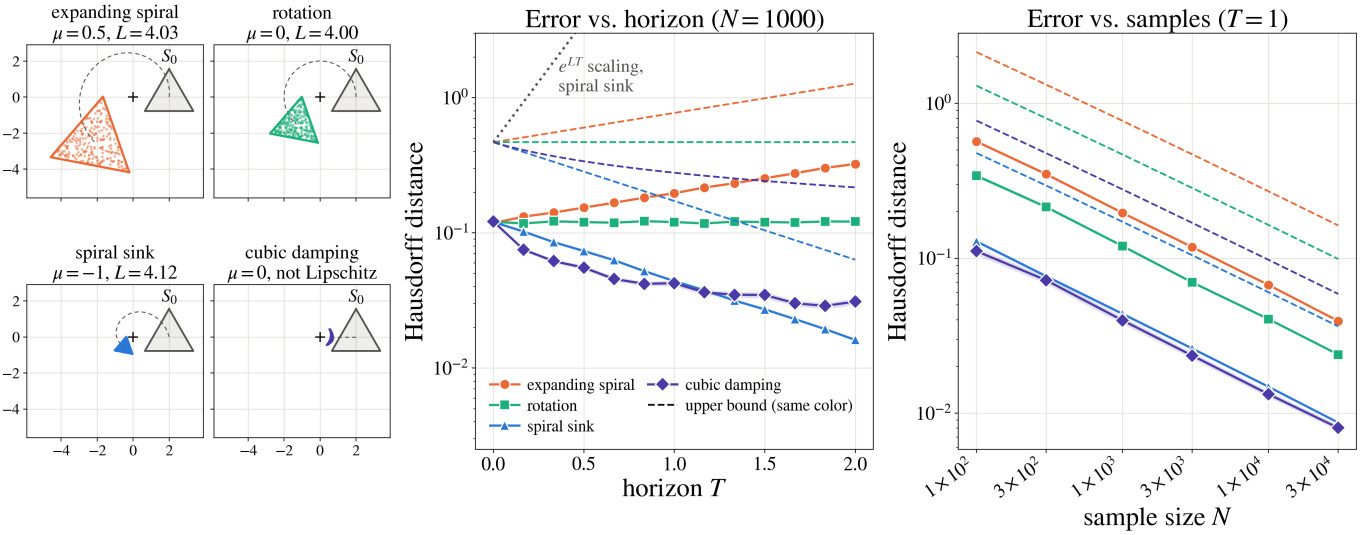


Fig. 3. Four vector fields on the equilateral triangle of area π. Left: S_0, S_T at $T = 1$ with 250 endpoints, and the centroid trajectory. Middle: mean Hausdorff error against T at $N = 1000$. Right: error against N at $T = 1$. Bands: 95% confidence intervals. Dashed: the upper bound of Theorem 1 and Corollary 1 solved for r, with $e^{\mu T}$ for the linear fields and a Lipschitz bound for φ_T on S_0 for the cubic field. Dotted: the growth e^{LT} that a two-sided Lipschitz bound predicts for the spiral sink.

radial eigenvalues $(1 + 2T\|x\|^2)^{-1/2}$ and $(1 + 2T\|x\|^2)^{-3/2}$. Thus $L_T := (1 + 2Td_0^2)^{-1/2}$, with $d_0 := d(0, S_0) \approx 0.954$, is a Lipschitz bound. Substituting L_T for $e^{\mu T}$ is justified by Remark 4 and gives the decreasing dashed curve; the measured error decreases faster still, by the factor 0.256 at $T = 2$ against 0.464, because the flow contracts the radial direction more strongly than the tangential one. The sweep over N at $T = 1$ (right) shows that the dynamics shift the curves and leave their fitted slopes similar (approximately -0.47 for all four fields); for the three linear fields the shift is the factor $e^{\mu T}$.

C. Sample Complexity under Contraction

We keep F_{-1} and fix the accuracy $r = 0.03$. Along one i.i.d. sequence per trial we record the first N for which $d_H(S_T, \{Y_1, \ldots, Y_N\}) \le r$, with all integer budgets up to 64 and a geometric grid of ratio $2^{1/8}$ thereafter, and use its empirical 95% quantile to estimate sample complexity. Theorem 1 bounds the population quantile; the empirical quantile also reflects finite-trial variability and the grid in N. Since φ_T is a rotation composed with the scaling $e^{\mu T}$, $d_H(S_T, \{Y_i\}_{i\le N}) = e^{\mu T} d_H(S_0, \{X_i\}_{i\le N})$, so one error curve per trial yields this number for every horizon, and

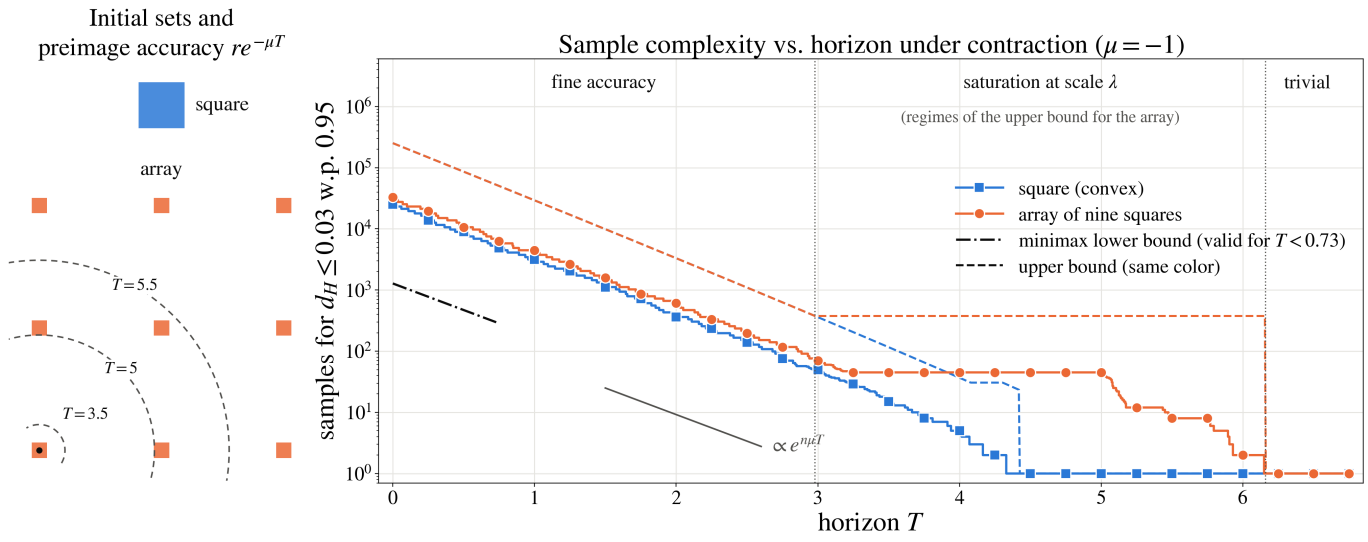


Fig. 4. Sample complexity against the horizon under the spiral sink F_{-1}. Left: the two initial sets to scale; the dashed arcs have radius $re^{-\mu T}$, $r = 0.03$, around a point of a corner piece. Right: samples needed for $d_H(S_T, \widehat{S}_N) \le r$ in 95% of 200 trials, on a grid of step 0.005 in T (solid steps) and at the horizons $T \in \{0, 0.25, \dots\}$ (markers); the upper bound (dashed); and the minimax lower bound (9) (dash-dotted), drawn only where it applies, $r < e^{\mu T} R/16$, that is, $T < 0.73$. Vertical lines mark the horizons where the preimage scale reaches λ and where the one-sample bound begins.

we evaluate it on a grid of step 0.005 in T. We compare two initial sets (Fig. 4, left): a square, which is convex with $(\kappa, \lambda) = (1/4, 0.886)$, and an array of nine squares of side 0.59 on a lattice of pitch 4.73, which is $(1/4, 0.295)$-standard by Corollary 3(ii) and is an instance of a disconnected initial set.

For $T \le 2.75$, $r \le 2e^{\mu T}\lambda$ for both sets, and their sample complexity decays like $e^{n\mu T}$: the fitted rates are -2.08 for the square and -2.02 for the array against $n\mu = -2$, from about 3×10^4 samples at $T = 0$ to about 10^2 at $T = 2.75$. The upper bound is parallel to the data and a factor 5 to 11 above them; the minimax lower bound (9) with $\kappa = \frac{1}{4}$, which applies only while $r < e^{\mu T} R/16$, that is, for $T < 0.73$, lies a factor of 18 to 26 below the empirical curves on that interval. The lower curve concerns the larger family with standardness scale $\lambda_{\mathrm{lb}} = \min\{\lambda, 3R/32\}$; it is not a lower bound for either fixed initial set or for the smaller family with its original, larger λ. Contraction reduces the empirical sampling burden at a rate consistent with Theorem 1.

At $T = 2.98$, the preimage scale $\frac{1}{2}e^{-\mu T} r$ of the array reaches λ, and its bound saturates at 376 samples. The empirical sample complexity saturates as well and equals 45 for every $T \in [3.25, 5]$. To explain this plateau, let ℓ be the side of a piece and $p = 8\ell$ be the pitch. For $T \in [3.5, 4.995]$, the accuracy pulled back to the initial set, $re^{-\mu T} \in [0.99, 4.43]$, exceeds the diagonal 0.84 of a piece, so a sample inside a piece covers the whole piece; it is also below $p - \ell/2 \approx 4.431$, the distance from the center of any piece to the nearest other piece. On this interval, therefore, the reachable set is covered exactly when every piece has been hit, and the 95% quantile of the corresponding coupon-collector time for nine equally likely pieces is 44. At $T = 5$ the pulled-back accuracy is $4.452 > 4.431$, so this sufficient condition for the coupon-collector equivalence no longer holds beyond $T \approx 4.995$. The square, in contrast, keeps improving and needs a single sample from $T = 4.33$ on, consistent with Corollary 1 and case (3) of Theorem 1, which guarantee one sample for $T \ge \log(\mathrm{diam}(S_0)/r) = 4.43$. For the array the one-sample bound starts at $T = 6.16$ in the bound and at $T = 6.15$ in the data. Between $T = 5$ and $T = 6.16$ a sample starts to cover neighboring pieces and the empirical sample complexity falls below the plateau in steps, which (5) does not follow; this gap between the empirical plateau and the saturated bound is listed among the open problems of Section V.

TABLE III
FITTED CONVERGENCE SLOPES AND 95% CONFIDENCE INTERVALS FOR THE ROBOT-ARM EXPERIMENTS.

n	Uniform	Adversarial
4	-0.333	-0.422
	$[-0.342, -0.324]$	$[-0.438, -0.405]$
6	-0.253	-0.287
	$[-0.260, -0.247]$	$[-0.294, -0.279]$
8	-0.216	-0.234
	$[-0.223, -0.211]$	$[-0.240, -0.227]$

D. Dependence on the State Dimension

The final experiment examines dimension dependence and the empirical benefit of adaptive initial-state selection. We simulate vertical planar arms with $m \in \{2, 3, 4\}$ links in MuJoCo [27]. The state $x = (q, v) \in \mathbb{R}^n$, $n = 2m$, collects joint angles and velocities; a weak inverse-dynamics controller ($K_p = 0.01I$, $K_d = 0.005I$) tracks a sinusoidal reference, with the remaining parameters of Liu et al. [1]. The closed loop is time-varying. Remark 4 extends the upper-bound argument to this setting if a Lipschitz bound for φ_T on S_0 is available; we do not certify such a constant for the MuJoCo simulations. The initial set is the box $S_0 = [-0.1, 0.1]^n$,

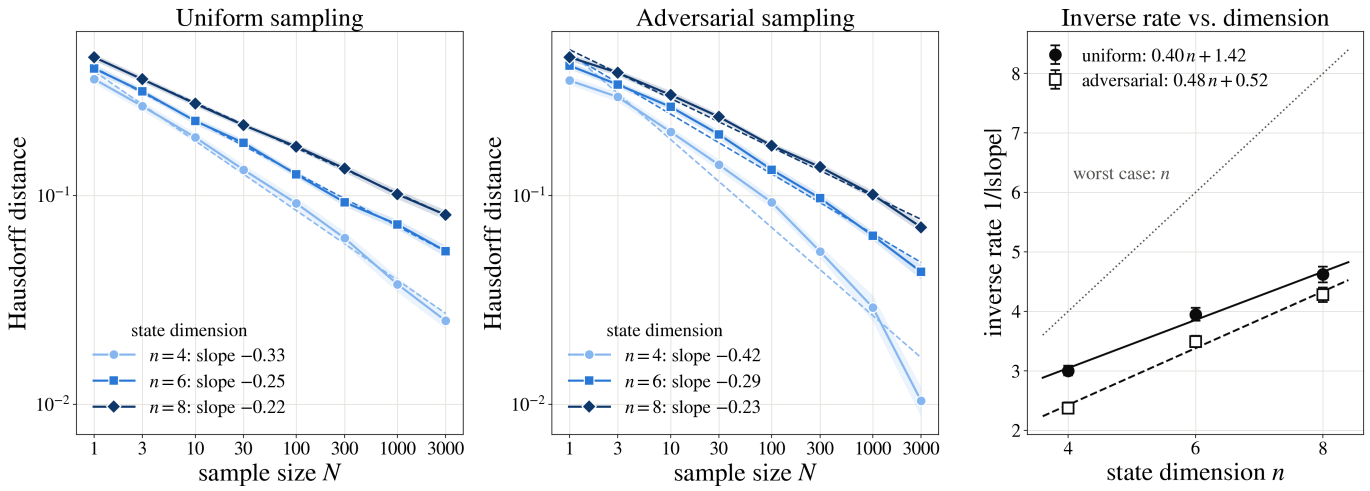


Fig. 5. Robot arm with $n/2$ links at $T = 1$. Left, middle: mean directed Hausdorff error of the convex hull of the endpoints against N under uniform and adversarial sampling (bands: 95% intervals over 30 seeds; dashed: fitted power laws). Right: inverse rate $1/|\text{slope}|$ against n with its linear fit and the bootstrap intervals of Table III; dotted: the worst-case exponent n.

sampled uniformly and propagated to $T = 1$; it is $(2^{-n}, 0.1)$-standard by Proposition 2(iii), so its geometry satisfies the upper-bound assumptions without the morphological opening used in Liu et al. [1]. The estimator is the convex hull of the endpoints, and the error is $\max_z d(z, \text{conv}\{Y_1, \dots, Y_N\})$ over 2000 reference endpoints, averaged over 30 seeds for $N \le 3000$. Finite reference sampling and numerical projection introduce approximation error, so the experiment shows a dimension-dependent degradation rather than a certified rate.

We compare i.i.d. uniform sampling with an adversarial heuristic inspired by Lew and Pavone [11] and approximating the update in Liu et al. [1, Algorithm 1]: half of the budget is drawn uniformly, and each sampled initial state is moved by a normalized step of length 0.05 in the direction $Q(Y_j - c)$ (with zero direction left unchanged), where c and Q are the mean and the regularized inverse covariance of the endpoints; the moved states are projected back onto S_0 and propagated again. This heuristic replaces the transpose of the flow Jacobian in the novelty gradient by the identity; it does not differentiate the simulator. These samples are neither independent nor identically distributed, so Theorem 2 does not apply to them and the comparison is empirical.

Table III reports slopes fitted over $N \in [1, 3000]$ and 95% confidence intervals from bootstrapping seed records while preserving shared random streams across budgets.

Under both schemes the empirical error is well approximated by a power law whose exponent decreases in magnitude as the dimension increases (Fig. 5, Table III). The fitted slopes are steeper than $-1/n$. This is compatible with a worst-case lower bound: the experiment uses specific systems, finite budgets, and an estimate of only one directed error. The adversarial samples also lie outside the i.i.d. model. With s_n the fitted slope in dimension n (Table III), the inverse fitted rate $1/|s_n|$ is approximately linear over the three tested dimensions: $0.40\,n + 1.42$ under uniform and $0.48\,n + 0.52$ under adversarial sampling (Fig. 5, right). Adversarial sampling lowers the inverse fitted rate over this range. Its mean error is 1 to 17% larger for the tested budgets $2 \le N \le 100$, where half of the budget goes to perturbed copies of the same states, and better by 59%, 21% and 13% for $n = 4, 6, 8$ at $N = 3000$, a gain that shrinks with n.

V. Conclusions and Open Problems

We have characterized the number of trajectory samples needed to recover a reachable set in Hausdorff distance within the i.i.d. endpoint model, in terms of the local volume density κ of S_0 and the one-sided Lipschitz constant μ of the vector field. Both quantities enter the upper and lower bounds through $(e^{\mu T} R/r)^n/(\rho\kappa)$; the two bounds agree up to the dimension-dependent factor $2 \cdot 4^n$ and logarithmic factors. For $n \ge 2$, under the scale and domain conditions of Theorem 2, the factor $1/(\rho\kappa)$ of the upper bound is matched for every $\kappa \le \kappa_n$; the lower bound, however, is minimax over instances rather than a pointwise bound for every initial set. The planar experiments support the predicted dependence on local geometry and flow distortion. The robot-arm experiments show dimension-dependent degradation over the tested range, without certifying an asymptotic rate.

Three gaps remain. The lower bound is proved only for $\kappa \le \kappa_n$, and its prefactor $2^{-(n+1)}$ differs from the prefactor 2^n of the upper bound, so the two bounds do not match uniformly in the dimension. In the saturated case, i.e., when $r > 2e^{\mu T}\lambda$, the upper bound (5) no longer depends on r, and a matching lower bound, presumably built from initial sets with many distant pieces of size λ, is missing; the nine-piece set of Section IV-C indicates what it should look like. Finally, a single constant μ uses the largest directional expansion rate; a bound that uses the Jacobian of the flow at the corners of S_0 would account for the anisotropy seen in Section IV-B. Beyond these gaps, the lower bound leaves adaptive and model-aware algorithms outside its scope (Remark 3).

REFERENCES

[1] J. Liu, I. Tabbara, H. Sibai, and E. Mallada, "On the limits of sampling-based reachability: Geometry, dynamics, and sample complexity," in *Conference on Robot Learning (CoRL)*, 2026.

[2] P. D. Holmes, S. Kousik, B. Zhang, D. Raz, C. Barbalata, M. Johnson-Roberson, and R. Vasudevan, "Reachable sets for safe, real-time manipulator trajectory design," in *Proceedings of Robotics: Science and Systems*, 2020.

[3] Y. Meng, D. Sun, Z. Qiu, M. T. B. Waez, and C. Fan, "Learning density distribution of reachable states for autonomous systems," in *Conference on Robot Learning*. PMLR, 2022, pp. 124–136.

[4] R. Ivanov, T. Carpenter, J. Weimer, R. Alur, G. Pappas, and I. Lee, "Verisig 2.0: Verification of neural network controllers using Taylor model preconditioning," in *International Conference on Computer Aided Verification*. Springer, 2021, pp. 249–262.

[5] J. Wu, H. Zhang, and Y. Vorobeychik, "Verified safe reinforcement learning for neural network dynamic models," *Advances in Neural Information Processing Systems*, vol. 37, pp. 117 762–117 783, 2024.

[6] S. Bansal, M. Chen, S. Herbert, and C. J. Tomlin, "Hamilton–Jacobi reachability: A brief overview and recent advances," in *2017 IEEE 56th annual conference on decision and control (CDC)*. IEEE, 2017, pp. 2242–2253.

[7] M. Chen and C. J. Tomlin, "Hamilton–Jacobi reachability: Some recent theoretical advances and applications in unmanned airspace management," *Annual Review of Control, Robotics, and Autonomous Systems*, vol. 1, no. 1, pp. 333–358, 2018.

[8] A. Girard, "Reachability of uncertain linear systems using zonotopes," in *Hybrid Systems: Computation and Control*, 2005.

[9] A. B. Kurzhanski and P. Varaiya, "Ellipsoidal techniques for reachability analysis," in *Hybrid Systems: Computation and Control*, 2000.

[10] L. Liebenwein, C. Baykal, I. Gilitschenski, S. Karaman, and D. Rus, "Sampling-based approximation algorithms for reachability analysis with provable guarantees," in *Proceedings of Robotics: Science and Systems*, 2018.

[11] T. Lew and M. Pavone, "Sampling-based reachability analysis: A random set theory approach with adversarial sampling," in *Proceedings of the 2020 Conference on Robot Learning*, vol. 155. PMLR, 2021, pp. 2055–2070.

[12] T. Lew, L. Janson, R. Bonalli, and M. Pavone, "A simple and efficient sampling-based algorithm for general reachability analysis," in *Learning for Dynamics and Control Conference*. PMLR, 2022, pp. 1086–1099.

[13] A. Devonport, F. Yang, L. El Ghaoui, and M. Arcak, "Data-driven reachability analysis with Christoffel functions," in *2021 60th IEEE Conference on Decision and Control (CDC)*. IEEE, 2021, pp. 5067–5072.

[14] M. Selim, A. Alanwar, S. Kousik, G. Gao, M. Pavone, and K. H. Johansson, "Safe reinforcement learning using black-box reachability analysis," *IEEE Robotics and Automation Letters*, vol. 7, no. 4, pp. 10 665–10 672, 2022.

[15] M. Ganai, Z. Gong, C. Yu, S. Herbert, and S. Gao, "Iterative reachability estimation for safe reinforcement learning," *Advances in Neural Information Processing Systems*, vol. 36, pp. 69 764–69 797, 2023.

[16] J. Liu and E. Mallada, "Recurrent control barrier functions: A path towards nonparametric safety verification," in *2025 IEEE 64th Conference on Decision and Control (CDC)*. IEEE, 2025, pp. 7721–7727.

[17] G. Williams, P. Drews, B. Goldfain, J. M. Rehg, and E. A. Theodorou, "Information-theoretic model predictive control: Theory and applications to autonomous driving," *IEEE Transactions on Robotics*, vol. 34, no. 6, pp. 1603–1622, 2018.

[18] C. Pan, Z. Yi, G. Shi, and G. Qu, "Model-based diffusion for trajectory optimization," in *Advances in Neural Information Processing Systems*, vol. 37, 2024.

[19] H. Xue, C. Pan, Z. Yi, G. Qu, and G. Shi, "Full-order sampling-based MPC for torque-level locomotion control via diffusion-style annealing," in *2025 IEEE International Conference on Robotics and Automation (ICRA)*. IEEE, 2025, pp. 4974–4981.

[20] W. Xiao, T.-H. Wang, C. Gan, R. Hasani, M. Lechner, and D. Rus, "SafeDiffuser: Safe planning with diffusion probabilistic models," in *International Conference on Learning Representations*, 2025.

[21] C. Pan, Z. Yi, G. Shi, and G. Qu, "Sampling-based methods for optimal control: Theory, algorithms, and applications," in *2025 IEEE 64th Conference on Decision and Control (CDC)*. IEEE, 2025, pp. 3775–3793.

[22] A. Devonport, F. Yang, L. El Ghaoui, and M. Arcak, "Data-driven reachability and support estimation with Christoffel functions," *IEEE Transactions on Automatic Control*, vol. 68, no. 9, pp. 5216–5229, 2023.

[23] T. Lew, R. Bonalli, and M. Pavone, "Convex hulls of reachable sets," *IEEE Transactions on Automatic Control*, vol. 70, no. 12, pp. 8195–8209, 2025.

[24] A. Cuevas and R. Fraiman, "A plug-in approach to support estimation," *The Annals of Statistics*, vol. 25, no. 6, pp. 2300–2312, 1997.

[25] A. Cuevas and A. Rodríguez-Casal, "On boundary estimation," *Advances in Applied Probability*, vol. 36, no. 2, pp. 340–354, 2004.

[26] F. Chazal, D. Cohen-Steiner, and A. Lieutier, "A sampling theory for compact sets in Euclidean space," *Discrete & Computational Geometry*, vol. 41, no. 3, pp. 461–479, 2009.

[27] E. Todorov, T. Erez, and Y. Tassa, "MuJoCo: A physics engine for model-based control," in *IEEE/RSJ International Conference on Intelligent Robots and Systems*, 2012, pp. 5026–5033.

[28] W. Lohmiller and J.-J. E. Slotine, "On contraction analysis for non-linear systems," *Automatica*, vol. 34, no. 6, pp. 683–696, 1998.

[29] F. Bullo, *Contraction Theory for Dynamical Systems*. Kindle Direct Publishing, 2024, version 1.2. [Online]. Available: https://fbullo.github.io/ctds

[30] H. Federer, "Curvature measures," *Transactions of the American Mathematical Society*, vol. 93, no. 3, pp. 418–491, 1959.

APPENDIX A
PROOFS FOR SECTION III

A. Flow Bounds

Definition 3 (One-sided Lipschitz constant): A number $\mu \in \mathbb{R}$ is a one-sided Lipschitz constant of F on $\mathcal{X}$ if

$$\langle F(x) - F(y), x - y\rangle \le \mu \|x - y\|^2 \qquad \forall x, y \in \mathcal{X}.$$

The constant need not be the smallest admissible one.

Every L-Lipschitz field admits $\mu = L$, but a smaller, possibly negative, constant may be available for contracting fields [28], [29]. A field need not be globally Lipschitz to admit a finite μ: the cubic field $F(x) = -\|x\|^2 x$ admits $\mu = 0$. For $F(x) = Mx$ on $\mathbb{R}^n$, the smallest admissible constant is $\mu = \lambda_{\max}(\frac{1}{2}(M + M^\top))$. Thus $F(x) = -cx$ admits $\mu = -c$, the system $\dot{x}_1 = x_1$, $\dot{x}_2 = 0$ admits $\mu = 1$, and a rotation admits $\mu = 0$ although $L > 0$.

Lemma 3 (Flow bounds): Let Assumption 1 hold, let F be one-sided Lipschitz with constant $\mu \in \mathbb{R}$, and let S_0 be compact. Then

$$\|\varphi_T(x) - \varphi_T(y)\| \le e^{\mu T}\|x - y\|, \text{ for all } x, y \in S_0,$$

and $S_T = \varphi_T(S_0)$ is compact.

Proof of Lemma 3: Fix $x, y \in S_0$ and set $w(s) := \|\varphi(s, x) - \varphi(s, y)\|$ for $s \in [0, T]$. The integral form of the flow gives

$$\varphi(s, x) - \varphi(s, y) = x - y + \int_0^s \big[F(\varphi(\sigma, x)) - F(\varphi(\sigma, y))\big]\, d\sigma.$$

Where $w(s) > 0$, differentiating w^2 and using Definition 3 gives

$$\begin{aligned} w(s)w'(s) =& \big\langle \varphi(s, x) - \varphi(s, y),\, F(\varphi(s, x)) - F(\varphi(s, y))\big\rangle \\ \le& \mu\, w(s)^2, \end{aligned}$$

hence $w'(s) \le \mu w(s)$; by continuity the inequality holds for all s. Integrating over $[0, s]$ yields

$$w(s) \;\le\; w(0) + \mu \int_0^s w(\sigma)\, d\sigma.$$

Gronwall's inequality [29] yields

$$w(s) \;\le\; e^{\mu s} w(0), \qquad s \in [0, T].$$

Setting $s = T$ gives $\|\varphi_T(x) - \varphi_T(y)\| \le e^{\mu T}\|x - y\|$. In particular φ_T is continuous on the compact set S_0, so $S_T = \varphi_T(S_0)$ is compact. ∎

Remark 4 (Lipschitz endpoint maps): Let L_T be a Lipschitz constant of the endpoint map φ_T on S_0; for the one-sided Lipschitz flow, $L_T = e^{\mu T}$ is admissible. The local-mass, covering, and upper-bound arguments use only this Lipschitz property. They therefore remain valid for any endpoint map with a finite L_T, with L_T replacing $e^{\mu T}$. This includes well-posed time-varying dynamics whenever a bound on their endpoint map is available. If $L_T = 0$, the image is a singleton and one sample suffices.

B. Endpoint Mass and Covering

For reference, the local mass bound at the initial time reads as follows; Lemma 1 at $T = 0$ recovers it for $r \le \lambda$.

Lemma 4 (Initial local probability lower bound): Let $(S_0, F, P_0) \in \mathscr{F}^{\mathrm{std}}_{R,\mu,\kappa,\lambda,\rho}$. Then, for every $x \in S_0$ and every $r \in (0, \lambda]$, $P_0(\mathcal{B}_r(x)) \ge \rho\,\kappa\,(r/R)^n$.

Proof: The integrated density bound and (1) give

$$P_0(\mathcal{B}_r(x)) \;\ge\; \frac{\rho}{|S_0|}\,|\mathcal{B}_r(x) \cap S_0| \;\ge\; \frac{\rho\,\kappa\,\omega_n r^n}{\omega_n R^n} \;=\; \rho\,\kappa\Big(\frac{r}{R}\Big)^n.$$ ∎

Standardness is stated for radii up to λ, but it controls the local volume of S_0 at every scale, because a larger ball contains the ball of radius λ.

Lemma 5 (Local volume of the initial set at every scale): Let S_0 be (κ, λ)-standard. Then, for every $x \in S_0$ and every $s > 0$,

$$|\mathcal{B}_s(x) \cap S_0| \;\ge\; \kappa\,\omega_n \min\{s, \lambda\}^n.$$

Proof of Lemma 5: For $s \le \lambda$, the claim is Definition 1. For $s > \lambda$, the inclusion $\mathcal{B}_\lambda(x) \subseteq \mathcal{B}_s(x)$ and standardness at radius λ give

$$|\mathcal{B}_s(x) \cap S_0| \ge |\mathcal{B}_\lambda(x) \cap S_0| \ge \kappa\omega_n\lambda^n.$$ ∎

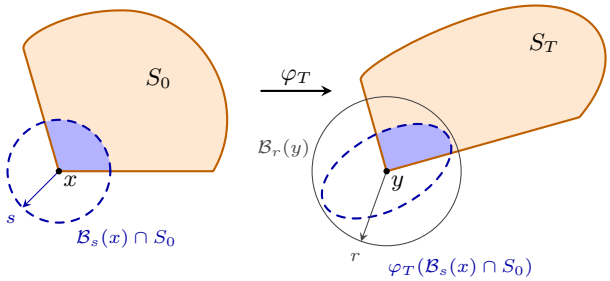


Fig. 6. Lemma 1: φ_T maps $\mathcal{B}_s(x) \cap S_0$ (shaded, left), $s = e^{-\mu T}r$, into $\mathcal{B}_r(y) \cap S_T$ (right), $y = \varphi_T(x)$. Dashed: the boundary of $\mathcal{B}_s(x)$ and its image; thin: $\mathcal{B}_r(y)$.

Proof of Lemma 1: Fix $y \in S_T$ and choose $x \in S_0$ with $y = \varphi_T(x)$. Set $s = e^{-\mu T}r$. By Lemma 3, every $z \in \mathcal{B}_s(x) \cap S_0$ satisfies

$$\|\varphi_T(z) - y\| \le e^{\mu T}\|z - x\| \le r.$$

Thus $\mathcal{B}_s(x) \cap S_0 \subseteq \varphi_T^{-1}(\mathcal{B}_r(y) \cap S_T)$; see Fig. 6. The push-forward identity, the integrated density bound, and Lemma 5 yield

$$\begin{aligned} P_T(\mathcal{B}_r(y) \cap S_T) &\ge P_0(\mathcal{B}_s(x) \cap S_0) \\ &\ge \frac{\rho}{\omega_n R^n}|\mathcal{B}_s(x) \cap S_0| \\ &\ge \rho\kappa\left(\frac{\min\{s, \lambda\}}{R}\right)^n. \end{aligned}$$

Substituting $s = e^{-\mu T}r$ proves (2). ∎

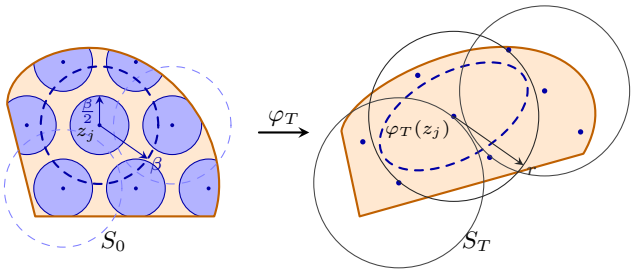


Fig. 7. Lemma 2. Left: a maximal β-separated set $\{z_j\}$ in S_0; the disjoint shaded sets $\mathcal{B}_{\beta/2}(z_j) \cap S_0$ bound M, and the dashed balls $\mathcal{B}_\beta(z_j)$ cover S_0. Right: the images $\varphi_T(z_j)$ form an r-cover of S_T, $r = e^{\mu T}\beta$; dashed: the image of $\mathcal{B}_\beta(z_j)$; thin: the balls of radius r.

Proof of Lemma 2: Fix $r > 0$ and set $\beta = e^{-\mu T}r$. The image under φ_T of any β-net in S_0 is an r-net in S_T, because φ_T is $e^{\mu T}$-Lipschitz. Hence

$$\mathcal{N}(S_T, r) \le \mathcal{N}(S_0, \beta). \tag{11}$$

Choose a maximal β-separated subset $\{z_1, \dots, z_M\}$ of S_0, where separation means $\|z_i - z_j\| > \beta$ for $i \ne j$. Compactness ensures that this set is finite. Maximality implies that it is a β-net: otherwise another point could be added. The balls $\mathcal{B}_{\beta/2}(z_j)$ are pairwise disjoint, so Lemma 5 gives

$$\begin{aligned} \omega_n R^n = |S_0| &\ge \sum_{j=1}^{M} |\mathcal{B}_{\beta/2}(z_j) \cap S_0| \\ &\ge M\kappa\omega_n \min\{\beta/2, \lambda\}^n. \end{aligned}$$

Consequently,

$$\mathcal{N}(S_0, \beta) \le M \le \frac{R^n}{\kappa \min\{\beta/2, \lambda\}^n}.$$

Combining this with (11) proves (3). Figure 7 illustrates the packing and covering steps. ∎

C. Upper Bound

Proof of Theorem 1: For cases (1) and (2), write $\varrho = \varrho_T(r)$ and $q_r = \rho\kappa(\varrho/R)^n$. By Lemma 1, every ball of radius $r/2$ centered in S_T has probability at least q_r. Choose an $r/2$-net $\{z_1, \dots, z_M\} \subseteq S_T$ of minimum cardinality. Lemma 2 and the inequality

$$\min\{e^{-\mu T}r/4, \lambda\} \ge \tfrac{1}{2}\min\{e^{-\mu T}r/2, \lambda\} = \varrho/2$$

give

$$M \le \frac{2^n R^n}{\kappa\varrho^n}. \tag{12}$$

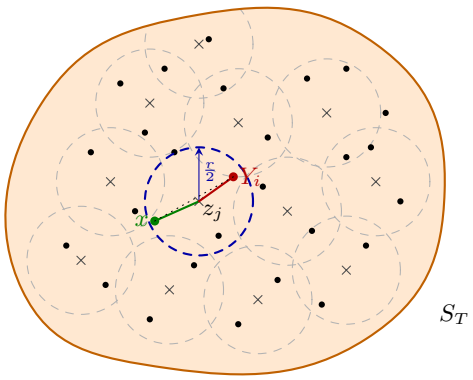


Fig. 8. Theorem 1: the centers z_j (crosses) of an $\frac{r}{2}$-net of S_T with their balls, and the endpoint samples (dots). When every net ball contains a sample, $d(x,\widehat{S}_N) \le \|x-z_j\| + \|z_j - Y_i\| \le r$ for every $x \in S_T$.

Let E_j be the event that $\mathcal{B}_{r/2}(z_j)$ contains no endpoint. Independence and the union bound imply

$$P_T^N\Big(\bigcup_{j=1}^{M} E_j\Big) \le M(1-q_r)^N \le Me^{-Nq_r}.$$

Both sample-size conditions are obtained from

$$N \ge \frac{1}{q_r}\left[\log\frac{2^n R^n}{\kappa\varrho^n} + \log\frac{1}{\delta}\right]$$

by substituting the relevant value of ϱ. Under either condition, (12) gives $Me^{-Nq_r} \le \delta$.

Outside the union of the bad events, every $x \in S_T$ has a net center z_j and an endpoint Y_i such that $\|x-z_j\| \le r/2$ and $\|z_j - Y_i\| \le r/2$. Since $Y_i \in \widehat{S}_N$,

$$d(x,\widehat{S}_N) \le \|x-Y_i\| \le \|x-z_j\| + \|z_j-Y_i\| \le r;$$

see Fig. 8.

For case (3), $\operatorname{diam}(S_T) \le e^{\mu T}D_0 \le r$. Almost surely, $Y_1 \in S_T \cap \widehat{S}_N$, so $d(x,\widehat{S}_N) \le \|x-Y_1\| \le r$ for every $x \in S_T$. ∎

Proof of Corollary 2: Theorem 1 provides an event of probability at least $1-\delta$ on which $\sup_{x\in S_T} d(x,\widehat{S}_N) \le r$. The outer-deviation condition $\widehat{S}_N \subseteq \mathcal{B}_\eta(S_T)$ means that $d(z,S_T) \le \eta$ for every $z \in \widehat{S}_N$. Therefore, on the same event,

$$\begin{aligned} d_H(S_T,\widehat{S}_N) &= \max\Big\{\sup_{x\in S_T} d(x,\widehat{S}_N),\ \sup_{z\in\widehat{S}_N} d(z,S_T)\Big\} \\ &\le \max\{r,\eta\}. \end{aligned}$$

∎

Proof of Corollary 1: First, $R \le D$: fix $x_0 \in S_0$. Every point of S_0 is within distance D of x_0, so $S_0 \subseteq \mathcal{B}_D(x_0)$, and $\omega_n R^n = |S_0| \le \omega_n D^n$. Hence $(R/D)^n \in (0,1]$.

Next, every ball centered in S_0 contains a scaled copy of S_0. Fix $x \in S_0$ and $s \in (0,D]$, and consider the homothety

$$H_x(z) := x + \frac{s}{D}(z-x), \qquad z \in \mathbb{R}^n.$$

For $z \in S_0$, convexity of S_0 gives $H_x(z) = (1-\frac{s}{D})x + \frac{s}{D}z \in S_0$, and

$$\|H_x(z) - x\| = \frac{s}{D}\|z-x\| \le \frac{s}{D}D = s.$$

Hence $H_x(S_0) \subseteq \mathcal{B}_s(x) \cap S_0$. Since H_x multiplies volumes by $(s/D)^n$ and $|S_0| = \omega_n R^n$,

$$\begin{aligned} |\mathcal{B}_s(x)\cap S_0| &\ge |H_x(S_0)| = \Big(\frac{s}{D}\Big)^n |S_0| \\ &= \Big(\frac{R}{D}\Big)^n \omega_n s^n. \end{aligned}$$

This is $((R/D)^n, D)$-standardness.

By this standardness, the instance belongs to $\mathscr{F}^{\mathrm{std}}_{R,\mu,\kappa',\lambda',\rho}$ with $(\kappa',\lambda') := ((R/D)^n, D)$, so Theorem 1 applies with (κ,λ) replaced by (κ',λ'), that is, with $\varrho_T(r)$ replaced by $\varrho'_T(r)$. For this pair,

$$\begin{aligned} \frac{1}{\rho\,\kappa'}\Big(\frac{R}{\varrho'_T(r)}\Big)^n &= \frac{1}{\rho}\Big(\frac{D}{\varrho'_T(r)}\Big)^n, \\ \log\Big(\frac{2^n R^n}{\kappa'\,\varrho'_T(r)^n}\Big) &= n\log\frac{2D}{\varrho'_T(r)}, \end{aligned}$$

so the bound of Theorem 1 becomes (6). ∎

D. Standard Sets and Inner Cones

This subsection collects the cone and inner-cone facts used in the lower-bound construction of Appendix A-E.

A set $K \subseteq \mathbb{R}^n$ is a *cone* if $tK \subseteq K$ for all $t > 0$. For a closed cone K, the *normalized solid angle* $\Theta(K) := |K \cap \mathcal{B}_1|/\omega_n \in [0,1]$ is the fraction of every ball centered at the apex that K occupies, because $|K \cap \mathcal{B}_r| = \Theta(K)\,\omega_n r^n$ by homogeneity; a planar wedge of opening θ has $\Theta = \theta/(2\pi)$. For $u \in \mathbb{S}^{n-1}$ and $\alpha \in (0,\pi/2]$, $K_\alpha(u) := \{v : \langle v,u\rangle \ge \|v\|\cos\alpha\}$ is the circular cone with axis u and half-angle α, and $\vartheta_n(\alpha) := \Theta(K_\alpha(u))$, which does not depend on u; in particular, the constant of (8) is $\kappa_n = \vartheta_n(\pi/4)$.

Definition 4 (Uniform inner-cone condition): Let $\mathscr{K}$ be a family of closed convex cones with nonempty interior and let $h > 0$. For $x \in S_0$ let $\mathscr{K}_h(x) := \{K \in \mathscr{K} : x + (K \cap \mathcal{B}_h) \subseteq S_0\}$ be the *admissible* cones at x. The set S_0 satisfies $\mathrm{UIC}(\mathscr{K},h)$ if $\mathscr{K}_h(x) \neq \varnothing$ for every $x \in S_0$. The *aperture* of $\mathscr{K}$ is $\vartheta(\mathscr{K}) := \inf_{K\in\mathscr{K}}\Theta(K)$. For the family $\mathscr{K} = \{K_\alpha(u)\}_{u\in\mathbb{S}^{n-1}}$ of circular cones of half-angle α we write $\mathrm{UIC}(\alpha,h)$; its aperture is $\vartheta_n(\alpha)$.

Inner cones: The next two lemmas combine the solid angle of a circular cone with the volume that an inner cone guarantees.

Lemma 6 (Solid angle of circular cones): For $n \ge 2$ and $\alpha \in (0,\pi/2]$,

$$\vartheta_n(\alpha) = \frac{(n-1)\,\omega_{n-1}}{n\,\omega_n}\int_0^\alpha \sin^{n-2}\phi\,d\phi \ \ge\ \Big(\frac{\sin\alpha}{1+\sin\alpha}\Big)^n, \tag{13}$$

with $\vartheta_2(\alpha) = \alpha/\pi$ and $\vartheta_3(\alpha) = (1-\cos\alpha)/2$. At $\alpha = \pi/2$ the cone $K_{\pi/2}(u)$ is the half-space $\{v : \langle v,u\rangle \ge 0\}$, so $\vartheta_n(\pi/2) = \frac{1}{2}$, while the lower bound in (13) equals 2^{-n}, the positive-reach constant.

Proof: Formula. Write $\xi = t\theta$ with $t = \|\xi\| \in [0,1]$ and $\theta \in \mathbb{S}^{n-1}$, and $\theta = \cos\phi\,u + \sin\phi\,\eta$ with the polar angle $\phi = \angle(\theta,u) \in [0,\pi]$ and η in the unit sphere of $u^\perp$, a copy of $\mathbb{S}^{n-2}$. Then $d\xi = t^{n-1}\,dt\,d\sigma_{n-1}(\theta)$ and

$d\sigma_{n-1}(\theta) = \sin^{n-2}\phi\, d\phi\, d\sigma_{n-2}(\eta)$, and $\theta \in K_\alpha(u)$ if and only if $\phi \le \alpha$. Hence, with $\sigma_{n-2}(\mathbb{S}^{n-2}) = (n-1)\omega_{n-1}$,

$$\begin{aligned}|K_\alpha(u)\cap\mathcal{B}_1| &= \int_{\mathbb{S}^{n-1}\cap K_\alpha(u)}\int_0^1 t^{n-1}\,dt\,d\sigma_{n-1}(\theta)\\ &= \frac{1}{n}\,\sigma_{n-1}\big(\mathbb{S}^{n-1}\cap K_\alpha(u)\big)\\ &= \frac{1}{n}\,\sigma_{n-2}(\mathbb{S}^{n-2})\int_0^\alpha \sin^{n-2}\phi\,d\phi\\ &= \frac{(n-1)\,\omega_{n-1}}{n}\int_0^\alpha \sin^{n-2}\phi\,d\phi,\end{aligned}$$

and dividing by ω_n gives the formula. With $\omega_1 = 2$, $\omega_2 = \pi$ and $\omega_3 = 4\pi/3$,

$$\begin{aligned}\vartheta_2(\alpha) &= \frac{2}{2\pi}\int_0^\alpha d\phi = \frac{\alpha}{\pi},\\ \vartheta_3(\alpha) &= \frac{2\pi}{4\pi}\int_0^\alpha \sin\phi\,d\phi = \frac{1-\cos\alpha}{2}.\end{aligned}$$

Lower bound. We fit a ball into $K_\alpha(u)\cap\mathcal{B}_1$. A ball centered at tu, $t>0$, lies in the cone if its radius is at most $t\sin\alpha$, the distance from tu to the boundary of the cone, and in $\mathcal{B}_1$ if, in addition, $t + t\sin\alpha \le 1$. The largest such ball has $t = 1/(1+s)$, where $s := \sin\alpha$; that is, it has center and radius

$$c := \frac{u}{1+s}, \qquad \varrho := \frac{s}{1+s} = s\,\|c\|.$$

Let $z = c+w$ with $\|w\| \le \varrho$. By the triangle inequality, $\|z\| \le \|c\| + \|w\| \le \frac{1}{1+s} + \frac{s}{1+s} = 1$. To check the cone condition, split $w = au + w_\perp$ with $a := \langle w, u\rangle$ and $w_\perp \perp u$, and let $b := \|w_\perp\|$, so that $a^2+b^2 = \|w\|^2$. Then $z = (\|c\|+a)u + w_\perp$, so

$$\langle z, u\rangle = \|c\| + a, \qquad \|z\|^2 = (\|c\|+a)^2 + b^2.$$

By definition, $z \in K_\alpha(u)$ means $\langle z,u\rangle \ge \|z\|\cos\alpha$. This holds as soon as

$$b\cos\alpha \;\le\; (\|c\|+a)\sin\alpha. \tag{14}$$

Indeed, (14) and $\sin\alpha > 0$ give $\|c\| + a \ge 0$, and squaring (14),

$$\begin{aligned}(\|c\|+a)^2 &= (\|c\|+a)^2\cos^2\alpha + (\|c\|+a)^2\sin^2\alpha\\ &\ge (\|c\|+a)^2\cos^2\alpha + b^2\cos^2\alpha \;=\; \|z\|^2\cos^2\alpha,\end{aligned}$$

so $\langle z,u\rangle = \|c\| + a \ge \|z\|\cos\alpha$.

It remains to prove (14). By the Cauchy–Schwarz inequality for the vectors $(b,-a)$ and $(\cos\alpha,\sin\alpha)$ of $\mathbb{R}^2$, and by $\varrho = \|c\|\sin\alpha$,

$$\begin{aligned}b\cos\alpha - a\sin\alpha &= \big\langle (b,-a), (\cos\alpha,\sin\alpha)\big\rangle\\ &\le \sqrt{a^2+b^2}\,\sqrt{\cos^2\alpha+\sin^2\alpha}\\ &= \|w\| \;\le\; \varrho \;=\; \|c\|\sin\alpha,\end{aligned}$$

which is (14) after moving $a\sin\alpha$ to the right.

Hence $\mathcal{B}_\varrho(c) \subseteq K_\alpha(u)\cap\mathcal{B}_1$, and

$$\vartheta_n(\alpha) = \frac{|K_\alpha(u)\cap\mathcal{B}_1|}{\omega_n} \;\ge\; \frac{|\mathcal{B}_\varrho(c)|}{\omega_n} = \varrho^n = \Big(\frac{\sin\alpha}{1+\sin\alpha}\Big)^n \qquad \blacksquare$$

Lemma 7 (Inner cones imply standardness): If S_0 is compact, satisfies $\mathrm{UIC}(\mathscr{K}, h)$, and $\vartheta(\mathscr{K}) > 0$, then S_0 is $(\vartheta(\mathscr{K}), h)$-standard.

Proof: For $x \in S_0$, $r \le h$ and $K \in \mathscr{K}_h(x)$, $x + (K\cap\mathcal{B}_r) \subseteq \mathcal{B}_r(x)\cap S_0$, so

$$\begin{aligned}|\mathcal{B}_r(x)\cap S_0| \;&\ge\; |K\cap\mathcal{B}_r| \;=\; \Theta(K)\,\omega_n r^n\\ &\ge\; \vartheta(\mathscr{K})\,\omega_n r^n.\end{aligned} \qquad \blacksquare$$

Proposition 1 (A ball satisfies the inner-cone condition): A closed ball $\mathcal{B}_{r_0}(c)$ satisfies $\mathrm{UIC}(\alpha, r_0\cos\alpha)$ for every $\alpha \in (0,\pi/2)$.

Proof: Fix $x \in \mathcal{B}_{r_0}(c)$, let $d := \|x-c\|$ and $u := (c-x)/d$ (any unit vector if $d=0$), and let v be a unit vector with $\phi := \angle(v,u) \le \alpha$. Let $\tau := r_0\cos\alpha$. The function $f(t) := \|x+tv-c\|^2 = t^2 - 2td\cos\phi + d^2$ is convex with $f(0) = d^2 \le r_0^2$. Since $g(d) := d^2 - 2\tau d\cos\alpha + \tau^2$ is convex on $[0, r_0]$,

$$\begin{aligned}f(\tau) &\le g(d) \le \max\{g(0), g(r_0)\}\\ &= \max\{r_0^2\cos^2\alpha,\; r_0^2\sin^2\alpha\} \le r_0^2.\end{aligned}$$

Hence $x + tv \in \mathcal{B}_{r_0}(c)$ for $t \in [0,\tau]$, i.e. $x + (K_\alpha(u)\cap\mathcal{B}_\tau) \subseteq \mathcal{B}_{r_0}(c)$. $\blacksquare$

E. Lower Bound

Throughout this subsection, $n \ge 2$, $y = (y_1, y') \in \mathbb{R}\times\mathbb{R}^{n-1}$, $\alpha \in (0,\pi/4]$ and $K := K_\alpha(-e_1) = \{w : \; w_1 \le 0,\; \|w'\| \le -w_1\tan\alpha\}$, so that $\Theta(K) = \vartheta_n(\alpha)$.

Lemma 8 (Cutting a tip): Let $q \in \mathbb{R}^n$ and $\varsigma > 0$. If $z \in q + K$ and $\|z-q\| \ge \varsigma$, then $z + K \subseteq (q+K)\setminus \mathring{\mathcal{B}}_\varsigma(q)$, where $\mathring{\mathcal{B}}_\varsigma(q)$ is the open ball.

Proof: As K is a convex cone, $z+K \subseteq q+K$. Two vectors of K make an angle of at most $2\alpha \le \pi/2$, so $\langle z-q, w\rangle \ge 0$ for $w \in K$, and

$$\begin{aligned}\|z+w-q\|^2 \;&=\; \|z-q\|^2 + 2\langle z-q, w\rangle + \|w\|^2\\ &\ge\; \|z-q\|^2 \;\ge\; \varsigma^2.\end{aligned} \qquad \blacksquare$$

The hard instances share a body Ω with conical tips at $\pm q$, $q := ae_1$, where Ω and a depend on $\bar R > 0$ and on the width of the tips. For thin tips, $\tan\alpha \le \frac12$, let $a := \frac65\bar R$ and

$$\begin{aligned}\Lambda &:= (q+K)\cap\{y_1 \ge 0\},\\ \Omega &:= \mathcal{B}_{\bar R}\cup\Lambda\cup(-\Lambda),\end{aligned}$$

a ball with two conical spikes. For wide tips, $\frac12 < \tan\alpha \le 1$, let $a := \bar R/\sin\alpha$, $b := \bar R\sin\alpha$ and

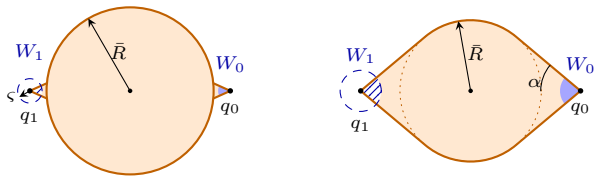
$$\begin{aligned}\Lambda &:= (q+K)\cap\{y_1 \ge b\},\\ \Omega &:= \mathrm{conv}\big(\mathcal{B}_{\bar R}\cup\{q,-q\}\big).\end{aligned}$$

In both cases Ω scales with $\bar R$. With $q_0 := q$ and $q_1 := -q$, the instances and their tip sectors are

$$S^{(i)} := \Omega\setminus\mathring{\mathcal{B}}_\varsigma(q_{1-i}), \qquad W_i := \Omega\cap\mathcal{B}_\varsigma(q_i), \qquad i = 0,1,$$

so $S^{(i)}$ keeps the tip at q_i and cuts off the other one (Fig. 9).

Lemma 9 (Shape of the body): (a) For thin tips, $\Omega \subseteq \mathcal{B}_{6\bar R/5}$ and $(q+K)\cap\{-\bar R/2 \le y_1 \le 0\} \subseteq \mathcal{B}_{\bar R}$. (b) For wide tips, $\Omega \subseteq q+K$, $\Omega = \mathcal{B}_{\bar R}\cup\Lambda\cup(-\Lambda)$ and $|\Omega| \le \frac{13}{5}\,\omega_n\bar R^n$.



thin tips, $\tan\alpha \le \frac{1}{2}$ wide tips, $\tan\alpha > \frac{1}{2}$

Fig. 9. Hard instances of Theorem 2 for thin tips (left) and wide tips (right). $S^{(0)}$ keeps the tip at q_0 and cuts off the tip at q_1 by $\mathring{\mathcal{B}}_\varsigma(q_1)$ (dashed); $S^{(1)}$ does the reverse. The instances differ on the sectors W_0 (shaded) and W_1 (hatched).

Proof: *(a)* Λ is the cone with apex q over a disk of radius $a\tan\alpha \le \frac{3}{5}\bar{R}$ in $\{y_1 = 0\}$, so its points have norm at most $\frac{6}{5}\bar{R}$. For y in the slab, $-\bar{R}/2 \le y_1 \le 0$ and $\tan\alpha \le \frac{1}{2}$ give

$$\begin{aligned}\|y'\| &\le (a-y_1)\tan\alpha \le \tfrac{1}{2}\left(\tfrac{6}{5}+\tfrac{1}{2}\right)\bar{R} = \tfrac{17}{20}\bar{R},\\ \|y\|^2 &\le \left(\tfrac{1}{4}+\tfrac{289}{400}\right)\bar{R}^2 \le \bar{R}^2.\end{aligned}$$

(b) Since $\sin\alpha = \bar{R}/a$, $q+K$ is the union of the rays from q through $\mathcal{B}_{\bar{R}}$; it is convex and contains $\mathcal{B}_{\bar{R}}$ and $-q$, hence Ω. As $0 \in \mathcal{B}_{\bar{R}}$ is the midpoint of $\pm q$, every point of Ω lies in $\mathrm{conv}(\mathcal{B}_{\bar{R}}\cup\{q\})$ or in $\mathrm{conv}(\mathcal{B}_{\bar{R}}\cup\{-q\})$: in $y = \lambda_1 z + \lambda_2 q - \lambda_3 q$ with $z \in \mathcal{B}_{\bar{R}}$ and $\lambda_2 \ge \lambda_3$, say, replace $\lambda_3(q-q)$ by $2\lambda_3 \cdot 0$. Let $y \in \mathrm{conv}(\mathcal{B}_{\bar{R}}\cup\{q\}) \setminus \mathcal{B}_{\bar{R}}$. If $y_1 < b$, then $y_1 < \|y\|\sin\alpha$, as $\|y\| > \bar{R}$, and $e := y/\|y\|$ satisfies

$$\langle q, e\rangle = \frac{a\, y_1}{\|y\|} < a\sin\alpha = \bar{R},$$

so the half-space $\{z : \langle z, e\rangle \le \bar{R}\}$ contains $\mathcal{B}_{\bar{R}}$ and q but not y, which is impossible; hence $y \in \Lambda$. Conversely, Λ is the cone with apex q over a disk of radius $(a-b)\tan\alpha = \bar{R}\cos\alpha$ in $\{y_1 = b\}$, which lies in $\mathcal{B}_{\bar{R}}$, so $\Lambda \subseteq \Omega$; by symmetry, $\Omega = \mathcal{B}_{\bar{R}} \cup \Lambda \cup (-\Lambda)$. This cone has height $a - b = \bar{R}\cos^2\alpha/\sin\alpha$, so

$$|\Lambda| = \frac{\omega_{n-1}}{n}\bar{R}^n\frac{\cos^{n+1}\alpha}{\sin\alpha} \le \frac{8\,\omega_{n-1}}{5n}\bar{R}^n \le \frac{4}{5}\omega_n\bar{R}^n,$$

because, for $\tan\alpha > \frac{1}{2}$ and $n \ge 2$,

$$\frac{\cos^{n+1}\alpha}{\sin\alpha} \le \frac{\cos^3\alpha}{\sin\alpha} < \left(\frac{2}{\sqrt{5}}\right)^3\sqrt{5} = \frac{8}{5}$$

($\cos^3\alpha/\sin\alpha$ decreases in α, and $\tan\alpha = \frac{1}{2}$ gives $\cos\alpha = 2/\sqrt{5}$, $\sin\alpha = 1/\sqrt{5}$), and $n\omega_n \ge 2\omega_{n-1}$, as each half of the unit sphere projects onto the unit ball of $\mathbb{R}^{n-1}$. Hence

$$|\Omega| \le \omega_n\bar{R}^n + 2|\Lambda| \le \tfrac{13}{5}\omega_n\bar{R}^n,$$

which proves the conclusion. ∎

Lemma 10 (Two-tip instances): Let $R > 0$, $0 < \varsigma \le R/8$ and $\alpha \in (0, \pi/4]$, and choose $\bar{R}$ with $|\Omega| = \omega_n R^n + \vartheta_n(\alpha)\,\omega_n\varsigma^n$. Then for $i = 0, 1$: (i) $S^{(i)}$ is compact, $|\partial S^{(i)}| = 0$ and $|S^{(i)}| = \omega_n R^n$; (ii) $W_0 \cap W_1 = \varnothing$ and $|W_i| = \vartheta_n(\alpha)\,\omega_n\varsigma^n$; (iii) $S^{(i)}$ satisfies $\mathrm{UIC}(\alpha, 3R/32)$, hence it is $(\vartheta_n(\alpha), 3R/32)$-standard; (iv) $d_H(S^{(0)}, S^{(1)}) \ge \varsigma$.

Proof: As Ω scales with $\bar{R}$, the volume condition determines $\bar{R}$, and $\omega_n R^n \le |\Omega|$ together with Lemma 9 gives $\bar{R} \ge \frac{5}{6}R$ for thin tips and $\bar{R} \ge (\frac{5}{13})^{1/n}R > 0.62R$ for wide tips.

(ii) By symmetry consider $q_0 = q$. For thin tips, $\mathcal{B}_\varsigma(q) \subseteq \{y_1 \ge a - \varsigma\}$ with $a - \varsigma > \bar{R}$, since

$$a - \bar{R} = \frac{\bar{R}}{5} \ge \frac{R}{6} > \frac{R}{8} \ge \varsigma;$$

so it misses $\mathcal{B}_{\bar{R}}$ and $-\Lambda$ and meets Ω in $(q+K)\cap\mathcal{B}_\varsigma(q)$. For wide tips, $\mathcal{B}_\varsigma(q) \subseteq \{y_1 \ge b\}$ because

$$\varsigma \le \frac{R}{8} < \frac{\bar{R}}{\sqrt{2}} \le \frac{\bar{R}\cos^2\alpha}{\sin\alpha} = a - b,$$

and there Ω coincides with $q+K$, since $\Omega \subseteq q+K$ and $\Lambda \subseteq \Omega$. In both cases $W_0 = q + (K \cap \mathcal{B}_\varsigma)$, of volume $\vartheta_n(\alpha)\,\omega_n\varsigma^n$, and $W_0 \cap W_1 = \varnothing$ because $2a > 2\varsigma$.

(i) and (iv). Ω is a finite union of convex bodies, so $S^{(i)} = \Omega \setminus \mathring{\mathcal{B}}_\varsigma(q_{1-i})$ is compact with $\partial S^{(i)} \subseteq \partial\Omega \cup \partial\mathcal{B}_\varsigma(q_{1-i})$, and, by (ii), $|S^{(i)}| = |\Omega| - |W_{1-i}| = \omega_n R^n$. For (iv), $q_0 \in S^{(0)}$ while $S^{(1)}$ misses $\mathring{\mathcal{B}}_\varsigma(q_0)$.

(iii) By symmetry let $i = 1$, so that $S^{(1)}$ cuts off the tip at q_0, and let $h := 3R/32$. We find for every $x \in S^{(1)}$ a unit vector u with $x + (K_\alpha(u) \cap \mathcal{B}_h) \subseteq S^{(1)}$. If $x \in q_0 + K$ and $x + (K \cap \mathcal{B}_h) \subseteq \Omega$, then $u := -e_1$ works, because $\|x - q_0\| \ge \varsigma$ and Lemma 8 keeps $x + K$ outside $\mathring{\mathcal{B}}_\varsigma(q_0)$.

Thin tips. Here $\bar{R} \ge \frac{5}{6}R$ and $\alpha \le \pi/4$, so $\bar{R}\cos\alpha \ge \frac{5R}{6\sqrt{2}} > h$ and $\bar{R}/2 > h$. If $x \in \mathcal{B}_{\bar{R}}$, Proposition 1 gives a cone of height $\bar{R}\cos\alpha \ge h$ in $\mathcal{B}_{\bar{R}}$, which misses $\mathring{\mathcal{B}}_\varsigma(q_0)$. If $x \in \Lambda$ and $w \in K \cap \mathcal{B}_h$, then $x + w \in q_0 + K$ and $(x+w)_1 \ge -h \ge -\bar{R}/2$, so $x + w \in \Lambda$ or, by Lemma 9(a), $x + w \in \mathcal{B}_{\bar{R}}$; hence $u := -e_1$ works. If $x \in -\Lambda$, the mirror argument gives a cone in $\mathcal{B}_{\bar{R}} \cup (-\Lambda) \subseteq \{y_1 \le \bar{R}\}$, which misses $\mathring{\mathcal{B}}_\varsigma(q_0)$.

Wide tips. If $x_1 \ge b + h$, then $x + w \in q_0 + K$ and $(x + w)_1 \ge b$ for $w \in K \cap \mathcal{B}_h$, so $x + w \in \Lambda$ and $u := -e_1$ works. If $x_1 \le -(b + h)$, the mirror argument gives a cone in $-\Lambda \subseteq \{y_1 < 0\}$. If $|x_1| < b + h$, then $\|x\| \le \bar{R} + h$: either $x \in \mathcal{B}_{\bar{R}}$, or $x \in \pm\Lambda$ with $|x_1| = b + \tau$, $\tau \in [0, h)$, where the cross-section of Λ has radius at most $\bar{R}\cos\alpha$, so, as $b^2 + \bar{R}^2\cos^2\alpha = \bar{R}^2$ and $b \le \bar{R}$,

$$\begin{aligned}\|x\|^2 &\le (b+\tau)^2 + \bar{R}^2\cos^2\alpha\\ &= \bar{R}^2 + 2b\tau + \tau^2 \le (\bar{R}+\tau)^2.\end{aligned}$$

Let $u := -x/\|x\|$ (any unit vector if $x = 0$) and let v be a unit vector at angle $\phi \le \alpha$ from u. Since

$$\|x\|\sin\phi \le \frac{\bar{R} + h}{\sqrt{2}} < \bar{R},$$

the ray $x + tv$, $t \ge 0$, meets $\mathcal{B}_{\bar{R}}$ and leaves it at

$$t_{\mathrm{out}} = \|x\|\cos\phi + \left(\bar{R}^2 - \|x\|^2\sin^2\phi\right)^{1/2} \ge \bar{R}\cos\alpha \ge h;$$

the first term is at least $\bar{R}\cos\alpha$ if $\|x\| \ge \bar{R}$, the second if $\|x\| < \bar{R}$. By convexity, $x + tv \in \Omega$ for $t \in [0, t_{\mathrm{out}}]$, so $x + (K_\alpha(u) \cap \mathcal{B}_h) \subseteq \Omega$, and its points have $|y_1| < b + 2h \le a - \varsigma$, so they miss $\mathring{\mathcal{B}}_\varsigma(q_0)$. Here $\bar{R} > 0.62R$ gives

$$h < (\sqrt{2} - 1)\,\bar{R}, \qquad h \le \bar{R}\cos\alpha,$$
$$\varsigma + 2h \le \tfrac{5}{16}R < \bar{R}/\sqrt{2} \le a - b.$$

∎

Proof of Theorem 2: The function ϑ_n is continuous and strictly increasing with $\vartheta_n(0^+) = 0$ (Lemma 6) and $\vartheta_n(\pi/4) = \kappa_n$, so there is a unique $\alpha \in (0, \pi/4]$ with $\vartheta_n(\alpha) = \kappa$.

Fix $\varsigma \in (2re^{-\mu T}, R/8]$, chosen below independently of the estimator, let $S^{(0)}$, $S^{(1)}$, W_0 and W_1 be the sets of Lemma 10 translated by c, and let $C := S^{(0)} \cap S^{(1)}$, so that, up to null sets, $S^{(i)}$ is the disjoint union of C and W_i.

The body-radius estimates in Lemma 10 give $\bar{R} \le R(1 + \kappa 8^{-n})^{1/n}$ and, before translation, $\Omega \subseteq \mathcal{B}_{\sqrt{5}\bar{R}} \subseteq \mathcal{B}_{3R}$. Set $F(x) := \mu(x-c)$ on $\mathcal{X}$. Then $\varphi(t,x) = c + e^{\mu t}(x-c)$ and, for $i = 0, 1$ and $t \in [0,T]$, $\varphi(t, S^{(i)}) \subseteq \mathcal{B}_{3R\max\{1, e^{\mu T}\}}(c) \subseteq \mathcal{X}$. Thus both instances satisfy Assumption 1.

Let

$$p := \rho\,\kappa\,(\varsigma/R)^n \;\le\; \tfrac{1}{2}, \qquad P_0^{(i)} := (1-p)\,\mathrm{Unif}(C) + p\,\mathrm{Unif}(W_i).$$

By Lemma 10(i) and (iii), $S^{(i)}$ is compact with $|S^{(i)}| = \omega_n R^n$ and null boundary, and it is $(\kappa, 3R/32)$-standard; standardness persists when λ decreases. The law $P_0^{(i)}$ has density $p/|W_i| = \rho/|S^{(i)}|$ on W_i and, as $|C| = \omega_n R^n(1 - \kappa(\varsigma/R)^n)$ and $\rho \le 1$, density

$$\frac{1-p}{|C|} = \frac{1-\rho\,\kappa\,(\varsigma/R)^n}{1-\kappa\,(\varsigma/R)^n} \cdot \frac{1}{\omega_n R^n} \;\ge\; \frac{1}{|S^{(i)}|} \;\ge\; \frac{\rho}{|S^{(i)}|}$$

on C. Thus $P_0^{(i)}$ is absolutely continuous, and its density is positive on $S^{(i)}$. By standardness, every ball centered in $S^{(i)}$ meets $S^{(i)}$ in positive volume, so the support of $P_0^{(i)}$ is $S^{(i)}$. The law $P_0^{(i)}$ also satisfies the density bound of Definition 2, and it is the uniform law if $\rho = 1$. Hence each instance lies in $\mathscr{F}^{\mathrm{std}}_{R,\mu,\kappa,\lambda,\rho}$ whenever $\lambda \le 3R/32$.

By Lemma 10 (iv),

$$d_H\big(S_T^{(0)}, S_T^{(1)}\big) \;\ge\; e^{\mu T}\varsigma \;>\; 2r,$$

so, by the triangle inequality for Hausdorff distance, no estimate is within r of both targets.

Draw independent $B_j \sim \mathrm{Bernoulli}(p)$, $U_j \sim \mathrm{Unif}(C)$ and $V_j^{(i)} \sim \mathrm{Unif}(W_i)$, and set $X_j^{(i)} := U_j$ if $B_j = 0$ and $X_j^{(i)} := V_j^{(i)}$ otherwise. Each sequence is i.i.d. with law $P_0^{(i)}$. Let $\mathbb{P}$ denote the joint coupling law, and $P^{(i)}$ the marginal law of the endpoint data in instance i. On $E := \{B_1 = \cdots = B_N = 0\}$ the endpoint samples coincide, and so do the estimates. Let A_i be the event that the estimate computed from instance i has Hausdorff error greater than r. The separation of the targets gives $E \subseteq A_0 \cup A_1$. Since $\log(1-p) \ge -2p$ for $p \le \frac{1}{2}$,

$$\max_i P^{(i)}(A_i) \;\ge\; \tfrac{1}{2}\,\mathbb{P}(E) = \tfrac{1}{2}(1-p)^N \;\ge\; \tfrac{1}{2}e^{-2Np}.$$

At $\varsigma = 2re^{-\mu T}$,

$$\frac{1}{2p}\log\frac{1}{2\delta} \;=\; \frac{1}{2\rho\kappa}\Big(\frac{e^{\mu T}R}{2r}\Big)^n \log\frac{1}{2\delta} \;=\; N_{\mathrm{lb}}(r,\delta) \;>\; N.$$

By continuity some $\varsigma \in (2re^{-\mu T}, R/8]$ still has $2Np < \log\frac{1}{2\delta}$, and then $\max_i P^{(i)}(A_i) > \delta$. The same argument covers randomized estimators by giving both copies the same random seed, independent of the coupled data. ∎

Remark 5 (Range of κ): Lemma 8 needs $\alpha \le \pi/4$, which is why Theorem 2 stops at $\kappa_n = \vartheta_n(\pi/4)$. The range contains $(0, 2^{-n}]$: $\kappa_2 = \frac{1}{4}$, $\kappa_3 \approx 0.146$ and $\kappa_4 \approx 0.091$ against $2^{-n} = 0.25$, 0.125 and 0.0625. For $n \ge 4$, bounding $\sin^{n-2}\phi \ge \sin^{n-2}\phi\cos\phi$ in (13) gives

$$\kappa_n \;\ge\; \frac{(n-1)\,\omega_{n-1}}{n\,\omega_n}\int_0^{\pi/4}\sin^{n-2}\phi\cos\phi\,d\phi \;=\; \frac{\omega_{n-1}}{n\,\omega_n}\,2^{-(n-1)/2}.$$

Let $W_m := \int_0^{\pi/2}\sin^m\phi\,d\phi$; it decreases in m and $W_{m-1}W_m = \frac{\pi}{2m}$, so $W_m \le (\pi/(2m))^{1/2}$. With $\vartheta_n(\pi/2) = \frac{1}{2}$ in (13),

$$\frac{n\,\omega_n}{\omega_{n-1}} \;=\; 2(n-1)\,W_{n-2} \;\le\; 2(n-1)\Big(\frac{\pi}{2(n-2)}\Big)^{1/2} \;\le\; 2^{(n+1)/2},$$

where the last inequality holds at $n = 4$ and the ratio of consecutive left-hand sides is at most $\frac{4}{3} < \sqrt{2}$. Hence $\kappa_n \ge 2^{-(n-1)/2}\,2^{-(n+1)/2} = 2^{-n}$.

F. Standardness of the Main Classes of Sets

This subsection proves Proposition 2, which the main text and the experiments use; the lower-bound proof does not.

A convex polytope with nonempty interior is written irredundantly as

$$P = \{z :\; D_j(z) := \langle \nu_j, z\rangle - b_j \ge 0,\; j = 1,\dots,m\}, \quad (15)$$

with unit normals ν_j, facets $F_j := P \cap \{D_j = 0\}$, vertex set $V(P)$ and vertex cones $T_v := \{w : \langle \nu_j, w\rangle \ge 0 \text{ whenever } D_j(v) = 0\}$, $v \in V(P)$.

Proposition 2 (Classes of standard sets): Let $S_0 \subset \mathbb{R}^n$, $n \ge 2$, be compact.

(i) If S_0 is the closure of an open set A with $\mathrm{reach}(A^c) \ge r_0 > 0$, then S_0 is $(2^{-n}, r_0)$-standard.

(ii) If S_0 satisfies $\mathrm{UIC}(\alpha, h)$ (Definition 4), then S_0 is $(\vartheta_n(\alpha), h)$-standard, where

$$\vartheta_n(\alpha) \;\ge\; \Big(\frac{\sin\alpha}{1+\sin\alpha}\Big)^n, \qquad \vartheta_2(\alpha) = \frac{\alpha}{\pi}.$$

(iii) If $S_0 = P$ is a convex polytope as in (15), then S_0 is (κ_P, h_P)-standard with $\kappa_P := \min_{v\in V(P)}\Theta(T_v)$ and, with J ranging over the nonempty subsets of $\{1,\dots,m\}$,

$$h_P := \min\Big\{\min_{z\in P}\max_{j\in J} D_j(z) :\; \textstyle\bigcap_{j\in J} F_j = \varnothing\Big\} > 0. \quad (16)$$

The constant is optimal: $|\mathcal{B}_r(v_*) \cap P| = \kappa_P\omega_n r^n$ for a minimizing vertex v_* and all small r. If $S_0 = \bigcup_{\ell\le k} P_\ell$ for convex polytopes P_ℓ with nonempty interior, then S_0 is $(\min_\ell \kappa_{P_\ell}, \min_\ell h_{P_\ell})$-standard and $|\partial S_0| = 0$.

Positive reach: Item (i) is the following lemma.

Lemma 11 (Positive reach gives local volume): If S_0 is compact and is the closure of an open set A with $\mathrm{reach}(A^c) \ge r_0 > 0$, then $|\mathcal{B}_r(x) \cap S_0| \ge 2^{-n}\omega_n r^n$ for all $x \in S_0$ and $r \in (0, r_0]$.

Proof: First, every $x \in S_0$ lies in a closed ball $\mathcal{B}_{r_0}(c) \subseteq S_0$. To see this for $x \in A$, put $C = A^c$. If $d(x,C) \ge r_0$,

take $c = x$. Otherwise, let a be the unique nearest point of C and $u = (x-a)/d(x,C)$. The normal-ray property of positive reach [30, Thm. 4.8(6)] gives $d(a+tu,C) = t$ for $0 < t < r_0$. By continuity, $c = a + r_0 u$ has $d(c,C) = r_0$, so $\mathcal{B}_{r_0}(c) \subseteq \overline{A}$ and contains x. For $x \in \partial A$, approximate x by points of A and take a convergent subsequence of the corresponding centers, which lie in the compact set S_0. Let $d := \|x - c\|$ and $r \le r_0$. It suffices to find a ball of radius $r/2$ inside $\mathcal{B}_r(x) \cap \mathcal{B}_{r_0}(c)$. If $d < r/2$, the ball $\mathcal{B}_{r/2}(c)$ works. If $d \ge r/2$, let $q := x + \frac{r}{2}\frac{c-x}{d}$; for $z \in \mathcal{B}_{r/2}(q)$,

$$\|z - x\| \le \|z - q\| + \|q - x\| \le r,$$
$$\|z - c\| \le \|z - q\| + \|q - c\| \le \tfrac{r}{2} + \left(d - \tfrac{r}{2}\right) = d \le r_0. \quad \blacksquare$$

Polytopes: For a polytope P as in (15) and $x \in P$, let $J(x) := \{j : D_j(x) = 0\}$ be the active set, $T_x := \{w : \langle \nu_j, w\rangle \ge 0 \ \forall j \in J(x)\}$ the tangent cone, which is the vertex cone T_v when $x = v \in V(P)$, and $s_x := \min_{j \notin J(x)} D_j(x) > 0$. For $s \le s_x$, $P \cap \mathcal{B}_s(x) = (x + T_x) \cap \mathcal{B}_s(x)$: each D_j is 1-Lipschitz, so $D_j(z) \ge s_x - s \ge 0$ for $j \notin J(x)$, while $D_j(z) = \langle \nu_j, z - x\rangle$ for $j \in J(x)$.

Theorem 3 (Convex polytopes satisfy a uniform vertex-cone condition): Let P be as in (15), $S_0 := P$, $\mathscr{K}_P := \{T_v : v \in V(P)\}$ and h_P as in (16). Then $h_P > 0$, and every $x \in P$ has a vertex v with $x + (T_v \cap \mathcal{B}_{h_P}) \subseteq P$. Hence S_0 satisfies $\mathrm{UIC}(\mathscr{K}_P, h_P)$ and is (κ_P, h_P)-standard with $\kappa_P = \min_{v \in V(P)} \Theta(T_v)$, and $|\mathcal{B}_r(v_*) \cap P| = \kappa_P \omega_n r^n$ for a minimizing vertex v_* and $r \le s_{v_*}$.

Proof: $h_P > 0$. The family of index sets in (16) is finite and nonempty: if $D_j(z) = 0$ for all j and $p \in \operatorname{int} P$, then $D_j(z + t(p - z)) = tD_j(p) \ge 0$ for all $t \ge 0$, and P would contain a ray. For each admissible J, $\max_{j \in J} D_j$ attains its minimum on P, and the minimum is positive, since a zero would lie in $\bigcap_{j \in J} F_j = \varnothing$.

Vertex cones. Fix $x \in P$ and $J := \{j : D_j(x) < h_P\}$. If $J = \varnothing$, choose any vertex v. Otherwise $\bigcap_{j \in J} F_j \ne \varnothing$, since otherwise $h_P \le \max_{j \in J} D_j(x) < h_P$. In the latter case, this face contains a vertex v with $J \subseteq J(v)$. For $w \in T_v \cap \mathcal{B}_{h_P}$, $D_j(x + w) \ge D_j(x) \ge 0$ for $j \in J$ and $D_j(x + w) \ge D_j(x) - \|w\| \ge 0$ for $j \notin J$; hence $x + w \in P$. For $r \le s_{v_*}$, the local conical identity gives $|\mathcal{B}_r(v_*) \cap P| = |T_{v_*} \cap \mathcal{B}_r| = \kappa_P \omega_n r^n$. $\blacksquare$

Corollary 3 (Simplices and finite unions): (i) For a nondegenerate simplex Δ with heights η_i, h_Δ equals the inradius $\varrho_\Delta = (\sum_i \eta_i^{-1})^{-1}$, so Δ is $(\min_i \Theta(T_{v_i}), \varrho_\Delta)$-standard. (ii) If $S_0 = \bigcup_{\ell \le k} P_\ell$ for convex polytopes P_ℓ with nonempty interior, then S_0 is $(\min_\ell \kappa_{P_\ell}, \min_\ell h_{P_\ell})$-standard and $|\partial S_0| = 0$.

Proof: (i) With barycentric coordinates λ_i, $D_i = \eta_i \lambda_i$ and $\sum_i D_i/\eta_i = 1$, so $\max_i D_i \ge \varrho_\Delta$, with equality at the incenter. For a simplex, $\bigcap_{j \in J} F_j = \operatorname{conv}\{v_k : k \notin J\}$ is empty only for $J = \{0, \dots, n\}$, so (16) reduces to $h_\Delta = \min_z \max_i D_i(z) = \varrho_\Delta$; apply Theorem 3. *(ii)* Every $x \in S_0$ lies in some P_ℓ; Theorem 3 gives a cone T with $\Theta(T) \ge \kappa_{P_\ell}$ and $x + (T \cap \mathcal{B}_{h_{P_\ell}}) \subseteq P_\ell \subseteq S_0$. Apply Lemma 7; $\partial S_0 \subseteq \bigcup_\ell \partial P_\ell$ is null. Reflex vertices are therefore harmless: triangulate and apply (ii). $\blacksquare$

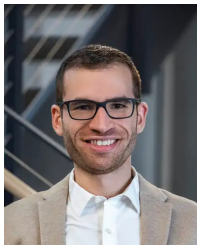
Proof of Proposition 2: For (i), apply Lemma 11 with $\kappa = 2^{-n}$ and $\lambda = r_0$. For (ii), Lemma 6 bounds $\vartheta_n(\alpha)$ below, and Lemma 7 converts $\mathrm{UIC}(\alpha, h)$ into $(\vartheta_n(\alpha), h)$-standardness. For (iii), Theorem 3 supplies (κ_P, h_P), and Corollary 3(ii) extends the constants to finite unions with $|\partial S_0| = 0$. $\blacksquare$



Jixian Liu is currently pursuing the Ph.D. degree with the Data Science and AI Institute, Johns Hopkins University, Baltimore, MD, USA. He received the B.Sc. degree from the School of Physics, Xi'an Jiaotong University, Xi'an, Shaanxi, China, in 2024. His research interests include robotics, control, and verifiable autonomous systems, with a focus on data-driven, learning-based and generative methods for safety verification.



Ihab Tabbara is currently pursuing the Ph.D. degree in Computer Science and Engineering at Washington University in St. Louis, St. Louis, MO, USA. He received the B.E. degree in Computer and Communication Engineering from the American University of Beirut, Beirut, Lebanon, in 2024. His research interests include robotics, machine learning, safe control, and formal methods.



Hussein Sibai is an Assistant Professor in the Department of Computer Science and Engineering at Washington University in St. Louis, St. Louis, MO, USA. He was previously a postdoctoral scholar at the University of California, Berkeley. He received the bachelor's degree in computer and communication engineering from the American University of Beirut, Beirut, Lebanon, and the master's and Ph.D. degrees in electrical and computer engineering from the University of Illinois Urbana-Champaign, Urbana, IL, USA, completing his Ph.D. in December 2021. His research interests include robotics, formal methods, control theory, and reinforcement learning. He received the Best Poster Award at HSCC 2018 and best paper nominations at HSCC 2017 and ATVA 2019. His honors include the Rambus Fellowship, the Ernest A. Reid Fellowship, the MAVIS Future Faculty Fellowship, and the ACM SIGBED gold medal in the graduate Student Research Competition at CPS Week 2021.



Enrique Mallada (S'09-M'13-SM'19) is an Associate Professor of Electrical and Computer Engineering at Johns Hopkins University. Prior to joining Hopkins in 2016, he was a Postdoctoral Fellow in the Center for the Mathematics of Information at Caltech from 2014 to 2016. He received his Ingeniero en Telecomunicaciones degree from Universidad ORT, Uruguay, in 2005 and his Ph.D. degree in Electrical and Computer Engineering with a minor in Applied Mathematics from Cornell University in 2014. Dr. Mallada was awarded the NSF CAREER award in 2018, the ECE Director's PhD Thesis Research Award for his dissertation in 2014, the Center for the Mathematics of Information (CMI) Fellowship from Caltech in 2014, and the Cornell University Jacobs Fellowship in 2011. His research interests lie in the areas of control, dynamical systems and optimization, with applications to engineering networks such as power systems and the Internet.